Mathematical modeling of transport phenomena during alloy solidification

C Beckermann
Department of Mechanical Engineering, The University of Iowa, Iowa City IA 52242

R Viskanta
School of Mechanical Engineering, Purdue University, West Lafayette IN 47907

Mathematical modeling of mass, momentum, heat, and species transport phenomena occurring during solidification of metal alloys is reviewed. Emphasis is placed on the incorporation of the effects of the solid structure and the interactions between the solid and liquid phases on a microscopic scale into a (macroscopic) model of the transport phenomena occurring at the system scale. Both columnar and equiaxed growth structures, as well as laminar convection of liquid and solid crystals are considered. The macroscopic conservation equations are introduced via a volume averaging approach and commonly made simplifications are examined. Basic constitutive relations for the phase interactions occurring in alloy solidification are presented. Recent progress in including nucleation, microsegregation, undercooling and other microscopic phenomena in the macroscopic equations is reviewed. The specific areas where future theoretical and experimental research is needed are identified.

LIST OF SYMBOLS

A	area
b	body force per unit volume
c	specific heat
C	concentration of a chemical species, i.e., mass fraction
$C_{D\varepsilon}$	generalized drag coefficient
$C_{i\varepsilon}$	generalized inertial coefficient
C_{io}	inertia coefficient
C_k	Kozeny constant
$C_{k\varepsilon}$	generalized Kozeny coefficient
d_s	mean particle length (diameter)
D	coefficient of diffusion tensor of a species in the multi-component mixture
g	equation of liquidus or solidus line [see Eq (37)]
h	average convective heat transfer coefficient
h_k	specific enthalpy of phase k
h_m	average convective mass transfer coefficient
I	unit tensor
j	species flux
J	total interfacial species transfer rate per unit volume
k	thermal conductivity tensor
$K^{(2)}$	second-order permeability tensor
L	latent heat of fusion
ℓ	diffusion length
M_i	interfacial momentum source due to surface tension
M	total interfacial momentum transfer rate per unit volume
n	index [see Eq (71)]
n	number density of crystals
$\dot{n}$	generation rate of crystals
n_k	outwardly directed unit normal vector on the interface of phase k
p	pressure
q	heat flux
Q	total interfacial heat transfer rate per unit volume
r_h	hydraulic radius
R	permeability ratio
R	resistance coefficient
Re	Reynolds number, [as defined by Eq (67)]

S	general source term in transport equation
S_v	interfacial area concentration
t	time
T	temperature
v	velocity
V	volume
w	velocity of the interface

Greek

Γ	interfacial mass transfer rate due to phase change
ε_k	volume fraction of phase k
γ	general diffusion coefficient
λ	mean dendrite arm spacing
μ	dynamic viscosity
ρ	mass average density
τ	shear stress
ϕ_k	a quantity of phase k
Φ_k	a quantity of phase k
X_k	phase function
Ψ_k	a quantity of phase k

Subscripts

a	aging
c	critical or crystal
D	drag
i	interfacial
k	phase k
ℓ	liquid
m	mixture
n	normal
s	solid or single
o	averaging volume
α	α-phase
β	β-phase

Superscripts

c	critical

© 1993 American Society of Mechanical Engineers

d	dissipative
j	species transfer rate
ℓ	linearized
q	heat transfer rate
t	dispersive flux or transpose of a tensor
Γ	due to phase change
τ	momentum transfer rate
$\wedge$	fluctuating component
$-$	interfacial average
$*$	effective or macroscopic

direction in solidification modeling research has emerged in the past five years that is concerned with the coupling of microscopic and macroscopic models. The aim of this research is to couple models of the basic nucleation and crystal growth mechanisms at the microscopic scale with macroscopic heat flow calculations in order to better predict the latent heat evolution and microstructural features on the

I. INTRODUCTION

Modeling of solidification processes is a rapidly expanding field and research activities have grown at an exponential rate. These efforts are not only aimed at improving traditional solidification processes such as casting of steel and non-ferrous alloys, but are continually stimulated by the development of new materials for which solidification constitutes the most effective and efficient manufacturing route. Recent examples include casting of metal-matrix composites (Rohatgi, 1988), production of materials with unique microstructures via solidification of undercooled melts (Sahm et al., 1986), and melt-textured growth of high-temperature superconducting crystals (Murphy et al., 1988). This paper focuses mainly on casting of metal alloys. Additional interest in solidification modeling has come from geologists who are concerned with magmatic crystallization (Huppert, 1990). Much of the recent progress has been made possible by the development of new numerical techniques and the widened availability of powerful computers (Voller et al., 1991). Nevertheless, it is still impossible to accurately predict the casting and the final solid properties of common iron alloys, a material known to mankind for millennia.

Solidification is a multi-disciplinary field encompassing material science and metallurgy, thermodynamics, fluid and solid mechanics, heat and mass transfer and other disciplines. One of the most challenging problems in solidification modeling is the complex interactions between physical phenomena occurring on different length scales ranging from atomic rearrangements, over single crystal-melt interactions, to heat extraction at the system level. This is illustrated in Fig 1. For example, it is not at all clear how to combine the known effects of convection on the growth of a single crystal (Glicksman et al., 1986) with the influence of macroscopic fluid motion on the evolution of crystal aggregates (i.e., "mushy zones") (Viskanta and Beckermann, 1987; Huppert, 1990) in a single model. The situation is even worse when different engineering disciplines are involved: no models are available that capture the fracture and break-off of microscopically small parts of a crystal due to solid stresses together with the ensuing solid (and induced liquid) motion and macroscopic transport. Another example is provided by the macrosegregation in continuous casting of steel caused by the deformation of the solid crystal skeleton formed during solidification (Lesoult, 1991).

While modeling of certain solidification processes and phenomena on a single scale and within a single discipline has matured to a considerable level of sophistication, a new
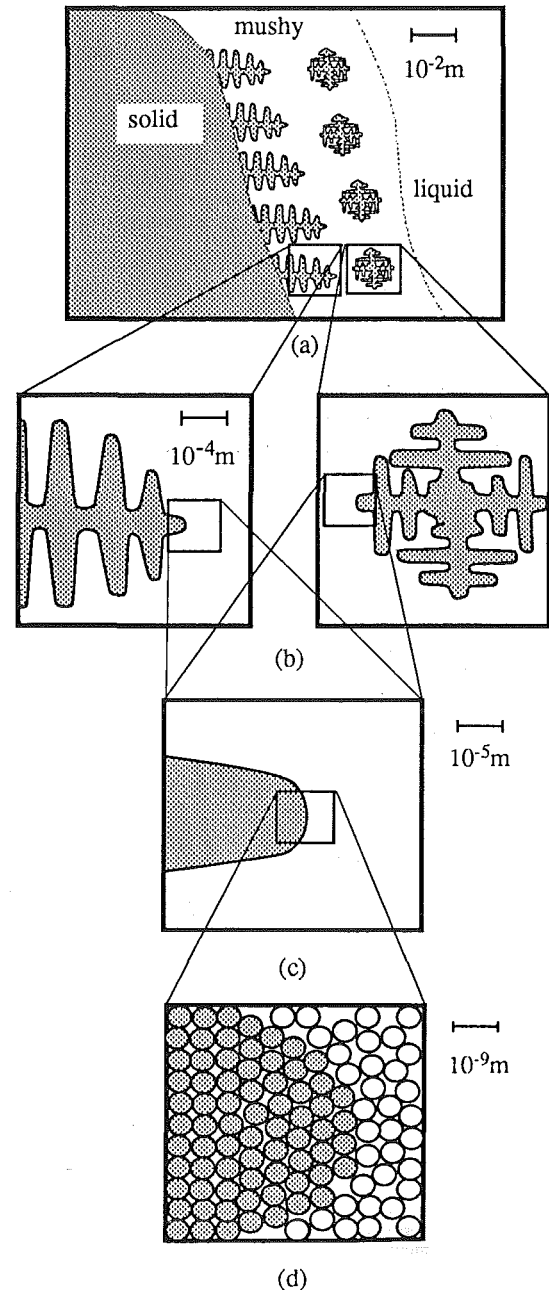

FIG 1. Illustration of physical scales and phenomena in dendritic solidification. (a) system (macroscopic) scale: mass, momentum, heat and species transport phenomena, cooling rate, latent heat evolution, grain patterns, macrosegregation, porosity, volume change; (b) grain scale: columnar and equiaxed crystals, local heat and species transfer, interfacial drag, spacings, coarsening; (c) interfacial scale: interface instabilities, capillarity, local equilibrium, dendrite tip undercooling and movement; (d) atomic scale: nucleation, interface structure (faceted, non faceted), atomic attachment kinetics.

system scale. This subject has been reviewed by Rappaz and Stefanescu (1988) and Rappaz (1989) and is also discussed in a recent textbook (Kurz and Fisher, 1989). The latest developments can be found in conference proceedings (Voller et al., 1991; Sekhar and Dantzig, 1991). Micro-macroscopic modeling is a new approach that does more justice to the coupled nature of solidification itself and also fosters multi-disciplinary research.

The purpose of this article is not to repeat the many reviews that have appeared in the literature on various aspects of alloy solidification, but to focus, from a thermal scientist's point of view, on recent attempts to create comprehensive macroscopic models of transport phenomena occurring during solidification of metal alloys that include more of the interactions with processes occurring on a microscopic scale. This approach is somewhat different from the micro-macroscopic work described by Rappaz (1989), in that more emphasis is placed on how the microscopic phenomena affect the macroscopic transport processes. The only (but important) coupling in the micro-macroscopic approach is through the latent heat evolution. The present paper makes no attempt at surveying the entire field. For example, important phenomena such as mold filling, turbulent convection and porosity formation are not considered. Many of the mathematical concepts may appear preliminary and can presently not be supported by experimental measurements. Furthermore, no applications of the models and results of calculations are presented. However, an account is provided of the many basic modeling issues left to be resolved.

The following section briefly introduces the basic physical phenomena occurring in alloy solidification. A general overview of important mathematical modeling developments is provided in Sec III. The fundamental model equations are derived in Sec IV. Section V reviews limiting forms of the conservation equations that are valid for stationary solid phases and minimize the need for special models (or constitutive relations) incorporating microscopic phenomena, but still provide good predictive capabilities for many macroscopic aspects of solidification. The inclusion of microscopic phenomena such as nucleation, micro-segregation, undercooling, and other phase interactions and non-equilibrium effects is discussed in Sec VI. A concluding discussion is presented in Sec VII.

II. BASIC ASPECTS OF ALLOY SOLIDIFICATION

Solidification of alloys differs in many respects from phase-change of pure substances and readers unfamiliar with the subject are referred to Kurz and Fisher (1989). Here, only a few basic concepts are introduced that are particularly relevant to the following discussion.

A typical equilibrium phase diagram for a fictitious eutectic-forming binary system X-Y (at constant pressure) is shown in Fig 2. Nucleation of small solid crystals occurs at

a temperature slightly below the liquidus temperature of an alloy of a given initial composition. As opposed to pure substances, liquid and solid can coexist in equilibrium over a range of temperatures up to the eutectic point. As the temperature of the solid-liquid interface is lowered, the compositions of the solid and liquid at the interface continually change. As indicated by the solidus line in Fig 2, on the left side of the eutectic point the solubility of species Y is much lower in the solid. This rejection of species causes the concentration in the liquid at the interface to increase along the liquidus line up to the eutectic composition. At the eutectic point two solid phases (α and β) of different composition form simultaneously and isothermally, such that the average composition is equal to the eutectic composition. In most practical casting processes the condition of phase equilibrium at the solid-liquid interface is met. Deviations from the phase diagram due to capillarity (i.e., curved interfaces), pressure, and kinetic (at high solidification rates) effects are discussed in textbooks (Flemings, 1974; Kurz and Fisher, 1989).

The formation of solid is basically governed by the temperature and species concentration gradients on each side of the solid-liquid interface. However, the *shape* of the interface is a much more complicated issue that also involves stability and interface curvature considerations, among others. Interesting accounts of recent research in this area can be found in Langer (1989) and Pines et al. (1990). Generally, alloy solidification is characterized by the presence of a large variety of microscopically complex interfacial structures. The macroscopic region over which solid-liquid interfaces exist is usually referred to as the mushy zone. It is of utmost importance in solidification modeling to take into account these interfacial structures, because they ultimately determine the final microstructure and, hence, many mechanical properties of the solidified alloy. Microstructure formation is strongly influenced by the alloy composition, the growth rate and the local temperature gradient. Fortunately, this can usually be reduced to the study of two classes of microstructure corresponding to eutectic and dendritic (off-eutectic) alloys (Kurz and Fisher, 1989). Each of these classes can be further subdivided into columnar (constrained) and equiaxed (unconstrained) structures. This is illustrated in Fig 3. In columnar growth
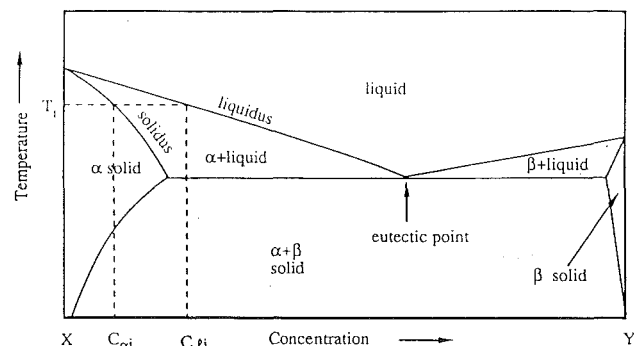
FIG 2.   Typical phase diagram for a binary alloy systems X-Y.

the solid is attached to a cooled wall and the speed of the crystal front is constrained by the movement of the isotherms. In equiaxed growth, on the other hand, the crystals grow radially into an undercooled melt and the latent heat is removed through the liquid (at least until impingement of the crystals).

Owing to the low mass diffusivity relative to the thermal diffusivity of metal alloys, solidification on a microscopic scale and, hence, microstructure formation is mainly controlled by the species (i.e., solute) concentration gradients on each side of the solid-liquid interface. On the *liquid* side of the interface, most of the solute is rejected laterally, in a direction perpendicular to the heat flow (e.g., between the dendrite arms or eutectic lamellae). However, it is important to realize that solute gradients must also exist in the liquid in *front* of the dendrite tip or the eutectic front for the solid to grow in a direction parallel to the heat flow. Furthermore, for equiaxed crystals completely surrounded by melt, the average interfacial temperature must be above the liquid temperature away from the crystal, in order to remove the latent (and sensible) heat (in columnar growth, the heat can be removed through the solid). In summary, there always exists a concentration gradient in the liquid through which the solute rejected during solidification is removed. Consequently, the interfacial concentration must be higher than the liquid concentration away from the interface. The difference between the concentration at the interface and some bulk value in the liquid is usually referred to as the solutal or constitutional undercooling (see Kurz and Fisher, 1989). The term "undercooling" stems from the practice to convert the two concentrations to temperatures via the liquidus line of the phase diagram. Thus, the melt is undercooled (i.e., it is in a metastable state) if the actual temperature at a point in

the liquid is below the liquidus temperature corresponding to the liquid concentration at that point. The *actual* temperature difference between the interface and some bulk value in the liquid is referred to as the thermal undercooling. Again, thermal undercooling plays usually only a minor role in microstructure formation, because of the high value of the thermal diffusivity of most metal alloys. Since the solute gradients in the liquid are confined to a very small region near the solid-liquid interface, convective influences on the solute transport have traditionally been neglected (Kurz and Fisher, 1989). A review of the influence of convection on microstructure formation is provided by Glicksman et al. (1986). Convection alters the microscopic concentration (and temperature) profiles and, hence, the shape of dendrites. In the limit of very slow cooling, convection may cause degeneration of an equiaxed dendritic crystal to a spheroid (Flemings, 1991). Spheroidal or "globulitic" crystals can also be found in highly inoculated castings where the small nuclei have no chance to develop a dendritic structure before they impinge upon each other.

Species inhomogeneities in the *solid* on a microscopic scale also have an important effect on the solidification phenomena. As the temperature is lowered, the concentration in the solid at the interface continually changes along the solidus line of Fig 2, and a microscopic concentration profile develops in the solid. This effect is termed microsegregation. The profile can change during solidification due to species diffusion (i.e., "back-diffusion"); however, owing to the small solid mass diffusivity of most metal alloys (the Fe-C system is an important exception), microsegregation usually persists in the solidified alloy. Sometimes, heat-treatment is applied to homogenize the microscopic solute variations. Microsegregation also influences the relative amounts of interdendritic precipitates (e.g., the eutectic phases). For a more complete description of microsegregation the reader is referred to textbooks (Flemings, 1974; Kurz and Fisher, 1989).

The above outlined microscopic phenomena manifest themselves in many interesting ways on a macroscopic (i.e., system) scale. Figure 4 illustrates the various structural zones that can develop in a casting (for simplicity, the process of filling of the mold that accompanies many casting processes is not shown). The nuclei that first appear at or near the cooled wall quickly develop into an outer equiaxed zone. Later, only those crystals survive that can grow parallel to the heat flow direction, leading to the formation of a columnar mushy zone. Once the superheat in the bulk liquid is dissipated, the melt ahead of the columnar dendrite tips becomes undercooled allowing equiaxed crystals to grow. The origin of the equiaxed crystals is not entirely clear, but most sources cite detachment of dendrite arms due to convection as the primary reason (Steube and Hellawell, 1992). Another theory claims that the equiaxed crystals simply grow from nuclei that were floating in the melt from the very beginning (Ohno, 1987). Obviously, equiaxed crystals are free to move in the melt until they pack and
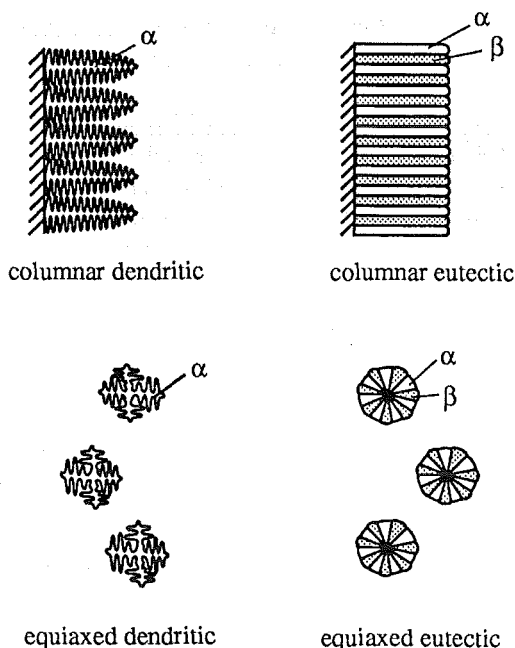
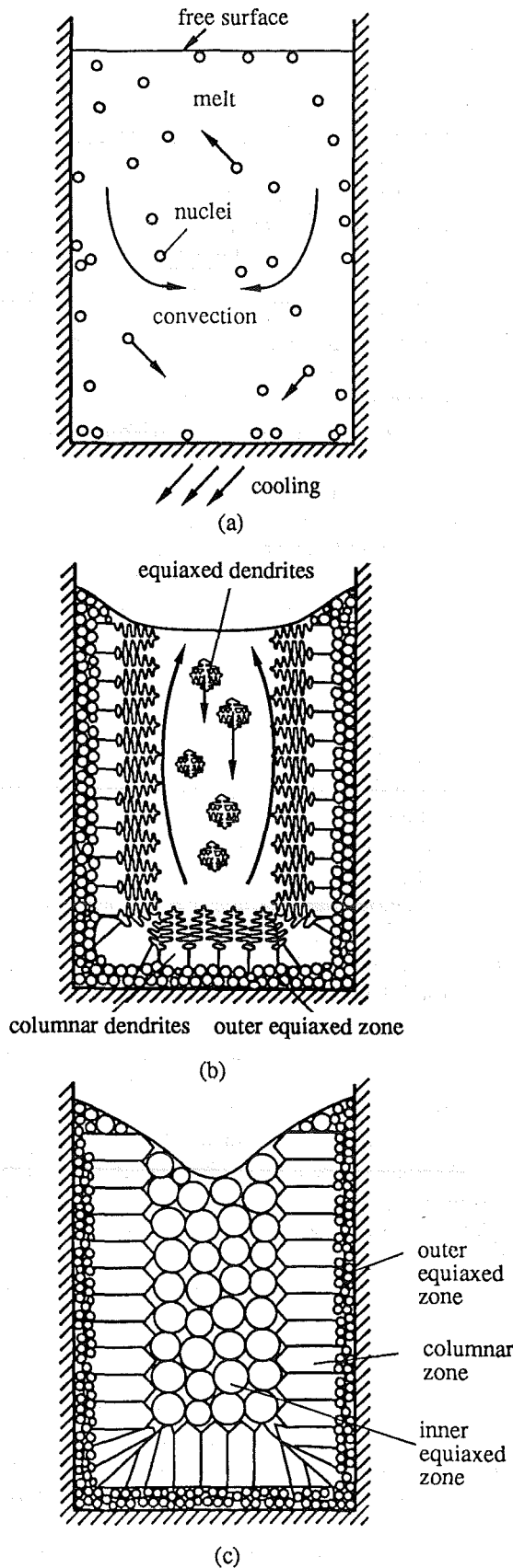FIG 3.   Microstructures in alloy solidification.

FIG 4. Development of structural zones in a casting (after Kurz and Fisher, 1989). (a) initial stage; (b) mediate stage; (c) final stage.

form the inner equiaxed zone. A finely grained equiaxed structure is often desirable in a casting and can be promoted through the use of inculants and electromagnetic stirring. A fully columnar structure can also be obtained, if the solidification and convection conditions are carefully controlled (Ohno, 1987).

The segregation of the chemical components at a solid-liquid interface during solidification also manifests itself on a macroscopic scale. Movement of either the liquid or the solid phase can induce compositional inhomogeneities on the system scale via advection, which is termed macro-segregation. A typical macrosegregation pattern of an alloy ingot is shown in Fig 5 (Flemings, 1974). Melt convection and solid movement, and their effects on macrosegregation, are discussed separately in the following. Generally, *melt flow* can be caused by (i) external forces such as imposed pressure gradients, rotation-translation of the mold or magnetic fields (forced convection), (ii) residual flow due to filling of the mold, (iii) density changes due to solidification as well as due to temperature and compositional changes within a phase, (iv) surface tension gradients at a free surface arising from temperature and/or concentration gradients (thermo-diffusocapillary flows), (v) the action of gravity on a density gradient (buoyancy driven flows), and (vi) drag forces from solid motion (see below). In the absence of external forces, buoyancy driven flows are often dominant (at least on earth). In addition, they are hard to quantify, influence and control. In alloys, density changes are due to both temperature and concentration so that the buoyancy driven flows are often called thermo-solutal or double-diffusive convection. Depending on the orientation relative to gravity, the thermal and solutal buoyancy forces either oppose or augment each other. For example, during solidification from the side the downward buoyancy force due to the horizontal temperature gradient is opposed or augmented by solutal buoyancy forces, depending on
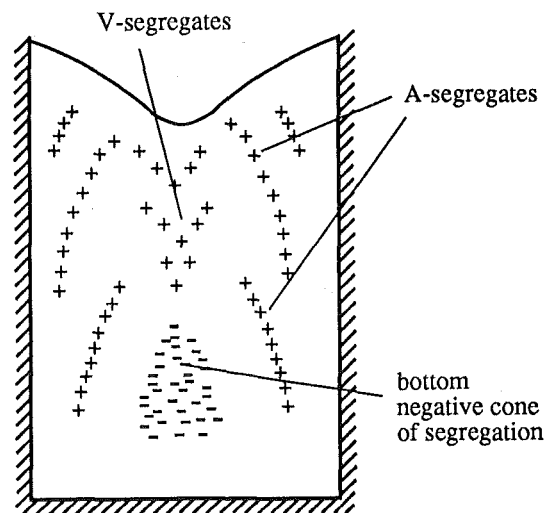

FIG 5. Macrosegregation pattern in a casting (after Flemings, 1974).

whether the lighter or the heavier component is rejected during solidification. Due to the much lower mass diffusivity relative to the thermal diffusivity of metal alloy melts, the liquid retains its composition. This may induce solutal layering in the liquid region, hydrodynamically stable stratifications or the formation of solutal plumes. Solutal layering has been shown to cause strong irregularities in the advance of a columnar dendritic growth front and even remelting (Beckermann and Viskanta, 1988). Solutal plumes are known to be responsible for channel segregates or freckles (Copley et al., 1970; Sample and Hellawell, 1984), which are shown as "+" signs in Fig 5. Convection of the melt in columnar dendritic solidification continues to be a very active research area, and detailed descriptions of the transport phenomena are available (Huppert, 1990; Incropera and Viskanta, 1992). Much less information is available on melt convection during equiaxed dendritic and eutectic solidification (e.g., Kato and Cahoon, 1985).

Movement of the solid phase, typically in the form of equiaxed crystals, can cause particularly severe macrosegregation (deGroh III and Laxmanan, 1988a). In addition, it is fundamental to the formation of equiaxed zones, the grain size distribution within equiaxed regions, and the columnar to equiaxed transition (Ohno, 1987). Free equiaxed crystals can move relative to the liquid due to the density difference between the solid and liquid phases in a gravitational field. Solid stresses (as in continuous casting), centrifugal forces, drag forces from melt convection, and other mechanical disturbances (Durand, 1992) can also induce solid motion. The settling of equiaxed crystals is known to be the cause of the bottom cone of negative segregation shown in Fig 5. The "kishing" of graphite flakes and the floating of various solid phases are important solid motion driven macrosegregation effects during solidification of Fe-C alloys (Flemings, 1974; Stefanescu et al., 1986). Extensive macrosegregation due to sedimentation has also been observed in solidification of undercooled Pb-Sn eutectic alloys (deGroh III and Laxmanan, 1988b). The crystals may be transported into a melt of different temperature and/or composition and may partially remelt. This causes the release of liquid that has the same composition as the remelted part of the crystal. This "history" effect has received very little research attention.

III. OVERVIEW OF MATHEMATICAL MODELS

The vast majority of alloy solidification models neglect melt convection, solid movement, and species redistribution on a macroscopic scale. Therefore, the only conservation equation that needs to be solved on the system scale is the heat diffusion equation:

$$\rho c \frac{\partial T}{\partial t} = \nabla \cdot (k \nabla T) + L \frac{\partial \varepsilon_S}{\partial t} . \tag{1}$$

The above equation is intended to be valid in the pure solid and liquid regions, as well as in the mushy zone where solid and liquid coexist. The so-called single-domain approach propagated by Eq (1) brings a significant advantage in a numerical solution, because a fixed grid can be used and there is no need to explicitly track the boundaries between the regions (Voller and Prakash, 1987). All thermophysical properties are some kind of mixture quantities that depend on the phase volume fractions. The last term on the right hand side of Eq (1) accounts for the latent heat release upon solidification. It is interesting to examine the origin and validity of Eq (1) more closely. The solid volume fraction, ε_S, actually represents an average value for a small volume element within the mushy zone. Hence, it varies continuously between 0 and 1. This volume element must be much larger than the microstructures and much smaller than the system for the solid fraction to be meaningful. Under typical solidification conditions, the system and interfacial structures are of the order of 10^0 to 10^{-1} m and 10^{-4} to 10^{-5} m, respectively, so that the size of the volume element can be around 10^{-2} to 10^{-3} m: about the size of a typical computational element. For example, in equiaxed solidification the volume element should contain several and not just a single crystal. Considering that an equiaxed crystal can have a diameter greater than 10^{-3} m, one wonders how meaningful a 100 by 100 computational grid in a square domain of 5 cm by 5 cm is (such a grid may be necessary to numerically resolve certain flow structures in more detailed models). Furthermore, it is shown in the following sections that Eq (1) assumes that the average temperatures of the solid and liquid in the volume element are the same; in other words, local thermal equilibrium is assumed. This opens the question how latent heat can be removed from equiaxed crystals which are completely surrounded by a melt that has the same average temperature as the crystal. In addition, if the average phase temperatures in the volume element are not the same as the solid-liquid interface temperature (as would be the case for thermal undercooling), the temperature T in Eq (1) should not be used in phase diagram relations.

One may regard the above issue as academic, because of the high thermal diffusivity of metal alloys. However, there are other microscopic phenomena that have a direct bearing on the utility of Eq (1). It was mentioned in Sec II that solidification on a microscopic scale (i.e., within the volume element) is governed by solute gradients and that the solid and liquid have different compositions in the mushy zone. On the other hand, it is well known that the phase enthalpies are strong functions of concentration (Poirier and Nandapurkar, 1988). It is seldom mentioned in the derivation of Eq (1) that the concentration dependencies are completely neglected. It has recently been shown for Pb-Sn alloys that predictions based on Eq (1) can differ by more than 10% from predictions based on an energy equation that includes the concentration dependencies (Schneider and Beckermann, 1991). Furthermore, the quantity L in Eq (1), representing the latent heat of fusion, is actually a difference in the

enthalpies between the solid and liquid phases averaged over the entire volume element (see Sec V.1). If one neglects, for example, the presence of a microscopic solute profile in the solid and evaluates the solid enthalpy at the interfacial concentration, an error of up to 2% is possible (Schneider and Beckermann, 1991). These issues were also investigated by Poirier et al. (1991). Other questions arise with regard to the thermophysical properties in Eq (1). The heat capacitance (ρc) is exactly given by the sum of the phase capacitances times the phase volume fractions. However, the mixture thermal conductivity k depends on the microstructure. A simple average of the phase thermal conductivities weighted by the volume fractions is only exact if the solid dendrites are cylinders of constant diameter growing in the direction of the heat flow. For equiaxed growth, for example, the mixture conductivity could be quite different (see Sec VI.2). This issue may be important considering that the solid and liquid thermal conductivities of many metals differ by more than a factor of two.

The solid volume fraction ε_S in Eq (1) must be calculated through a separate, "microscopic" model. These models are generally based on idealized solutions of the solute diffusion equations on a microscopic scale (Kurz and Fisher, 1989). For complete mixing of solute in the liquid, one can derive the well-known Lever rule and Scheil equation, which correspond, respectively, to the important limiting cases of complete mixing of solute within the solid on a microscopic scale and no solute diffusion in the solid at all. More sophisticated solid fraction models that take into account microscopic phenomena such as nucleation, undercooling of the melt, finite rate solute diffusion in the solid, coarsening, impingement and other microstructural dependencies have recently been reviewed by Rappaz (1989). They all contain one or more of the following ingredients:

- a nucleation model for the number density of equiaxed grains or columnar crystals; these models are often fully empirical and do not explicitly consider the actual physical phenomena leading to the formation and survival of grains; the grains are assumed to be remain stationary
- models for the shape of the grain (e.g., spherical) and the solid-liquid interfaces (e.g., the secondary dendrite arms, the dendrite tip, etc.); these models may include coarsening and impingement of interfaces
- direct or approximate solutions of the solute diffusion equation in the various microscopic geometries defined above; often, diffusion is assumed to be quasi-steady, limiting the models to low solidification rates; at the interface scale (see Fig 1), this results in so-called kinetic laws for the growth of the eutectic fronts or dendrite tips in an undercooled melt; for the solid, this results in predictions of microsegregation.

Micro-macroscopic models have been developed for a large variety of alloys and solidification modes and have provided predictions of cooling curves, recalescence, growth rates, grain sizes, microscopic solute profiles, and the solid fraction evolution. Impressive agreements with experimental measurements have been reported (Thevoz et al., 1989; Stefanescu et al., 1990; Goettsch and Dantzig, 1991). However, in the case of discrepancies, it is often not clear which particular model element is at fault, indicating a lack of systematic sensitivity and parametric studies. In addition, there remain at least three major areas where considerable additional research is needed:

- the influence of melt convection and the transport of small nuclei and equiaxed grains in the melt on the origin-survival of grains as well as on the their shape and growth
- the extension of the models to moderate and high solidification rates and the introduction of atomic attachment kinetics (see Fig 1)
- the modeling of mixed columnar-equiaxed structures, including the columnar to equiaxed transition (CET) in castings (Flood and Hunt, 1987).

In view of the limited utility of Eq (1), solidification models have been proposed that relax the assumption of a quiescent melt, but still allow for no solid transport. In addition to adding advective terms to the energy equation, one must solve a momentum and continuity equation for flow of the liquid in the mushy zone and the pure liquid region. Furthermore, convection causes redistribution of species on a macroscopic scale (i.e., macrosegregation), necessitating the solution of a species conservation equation. Finally, convection invalidates the above mentioned microscopic solid fraction models. Convection not only modifies the microscopic solute profiles, but also causes net flow of solute out of/into the volume element. The microscopic models used with Eq (1) all assume that solute transport on a microscopic scale is by diffusion only and that the mixture composition in the volume element remains constant (Kurz and Fisher, 1989; Rappaz, 1989). Modeling of alloy solidification with convection started with the work of Flemings and co-workers (1967, 1968a, and 1968b). They treated the mushy zone as a variable porosity porous medium and calculated macrosegregation due to flow driven by the solidification contraction only. The effect of gravity was first included by Mehrabian et al. (1970), who used Darcy's law to model the flow in the porous mushy zone. Temperature gradients were prescribed and the mixture concentration was assumed constant in the volume element. Ridder et al. (1978) also solved an energy equation, while Fujii et al. (1979) solved the coupled mass, momentum, energy, and species conservation equations for the mushy zone; however, convection in the pure liquid region was not considered. Szekely and Jassal (1978) and Ridder et al. (1978) solved for the first time the complete set of conservation equations for both the mushy and pure liquid zones. Mainly because the momentum equations for the mushy zone (Darcy's law) and the pure liquid region (Navier-Stokes equations) are of a different form, these researchers

utilized a multiple-domain approach, in which the transport equations for each region are written separately and coupled through certain interface conditions. Therefore, a numerical solution requires explicit tracking of the boundaries between each region and discretization of the equations on highly irregular domains.

More recently, macroscopic conservation equations have been derived that, like Eq (1), are equally valid in the mushy, solid and liquid regions and, hence, can be solved using a single-domain numerical solution procedure and a fixed grid. In one approach, mixture theory is utilized and the mushy zone is assumed to have certain macroscopic properties (Hills et al., 1983; Prantil and Dawson, 1983; Bennon and Incropera, 1987). In particular, Bennon and Incropera (1987) succeeded in casting their model equations into forms that are easily solved using standard numerical procedures (Patankar, 1982). Another approach is motivated by general theories of flow through porous media and of other multi-phase systems (Gray, 1975; Hassanizadeh and Gray, 1979a; Gray, 1983; Drew, 1983) and utilizes a formal volume averaging procedure (Beckermann, 1987; Beckermann and Viskanta, 1988; Ganesan and Poirier, 1990). The main difference between these approaches is that in volume averaging the macroscopic equations are rigorously derived from microscopic (exact) equations, while mixture theory *assumes* the validity of certain continuum relations on a macroscopic scale. Essentially, a formal averaging procedure shows how the various terms in the macroscopic equations arise and how the resulting macroscopic variables are related to the microscopic ones (Drew, 1983). According to Hassanizadeh and Gray (1990), the main disadvantage of mixture theory is that little connection is made with the microscopic reality. For example, virtually no mixture theory includes the interfacial area per volume and other interfacial properties. In solidification, this would imply the absence of important effects in the macroscopic equations, such as interfacial tension due to curvature, thermal and solutal undercooling, etc. If done carefully, both approaches yield the same macroscopic equations (Prescott et al., 1991). In order to simplify the solution of the conservation equations, thermal equilibrium between the phases is assumed [to yield an energy equation analogous to Eq (1)] and approximate relations are used for the macroscopic transport coefficients (Bennon and Incropera, 1987; Beckermann and Viskanta, 1988). Complications with the determination of the solid volume fraction are circumvented by assuming that within the small volume element the liquid is solutally well mixed and species diffusion in the solid is either complete or absent (Voller et al., 1989). The relevant equations governing alloy solidification with convection in the melt are provided in Sec V, together with a critical assessment of the assumptions made in their derivation and future research needs. Numerical solutions of the equations have yielded significant advances in understanding and simulating the effects of convection on alloy solidification. Physical phenomena predicted include development of an irregular liquidus front, remelting of

solid, development of flow channels in the mushy zone, and the establishment of certain macrosegregation patterns in the final solid (Prescott and Incropera, 1991). Recent reviews are available (Viskanta, 1990; Incropera and Viskanta, 1992; Huppert, 1990) and are not repeated here. Detailed comparisons with experiments are virtually nonexistent.

A relative new topic is the modeling of combined liquid and solid convection in alloy solidification, as may be present in coupled columnar and equiaxed growth. Several studies have addressed this problem by using averaged mixture equations and neglecting undercooling and grain growth kinetics. Because only a single (mixture) momentum equation is solved, some *a priori* assumption must be made about the relationship between the liquid and solid velocities. Voller et al. (1989) investigated the limiting case where the solid and liquid velocities are equal, which is valid for a highly dispersed solid phase. The viscosity of the mixture was enhanced with increasing solid fraction to simulate the formation of a coherent and rigid solid structure. When compared to a fully columnar structure, a more uniform macrosegregation pattern was predicted. A hybrid model was developed by Oldenburg and Spera (1992), where for a solid fraction below 0.5, the equal phase velocity/enhanced viscosity concept was utilized, while for $\varepsilon_s > 0.5$ a zero solid velocity model was used. The transition was accomplished through the use of certain switching functions. Flood et al. (1991) and Voller (1992), on the other hand, introduced the concept of a consolidation factor that specifies the relationship between the liquid and solid velocities. This factor is a simple linear function of the solid fraction and varies from unity for $\varepsilon_s \to 0$ (equal phase velocities) to zero at some given value of ε_s corresponding to a stationary solid. Prescott et al. (1992) switched from a zero solid velocity model with melt flow to an equal phase velocity model (with the viscosity equal to that of the liquid) for solid fractions below 0.01. In order to model recalescence, they introduced a solid fraction model that accounts for undercooling by specifying a certain decay rate of the undercooling from a maximum value. The undercooling model was calibrated using experimental data and produced fair agreement with temperature measurements for solidification of a Pb-Sn alloy. In general, the validity of the previous models cannot be established, due to a lack of suitable experimental data.

A different approach to the modeling of coupled columnar and equiaxed solidification is provided by the use of a so-called two-phase model (Ni and Beckermann, 1990, 1991; Prakash 1990a, 1990b). Separate volume averaged conservation equations are utilized for the solid and liquid phases. Therefore, no assumption about the relationship between the liquid and solid velocities needs to be made, and phenomena such as floating or settling of free solid grains can be modeled. In addition, the two-phase model distinguishes between the interfacial and bulk concentrations and temperatures, allowing for the prediction of liquid undercooling, microsegregation and other effects on a microscopic scale. Another key ingredient is the use of a

transport equation for the number density of grains, which allows for the inclusion of nucleation and the calculation of the local dimension of grains (Ni and Beckermann, 1990 and 1991). Prakash (1990a and 1990b) neglected the size influence of the grains on the transport and solidification phenomena. Beckermann and Ni (1992) presented results for the macrosegregation pattern and final grain size distribution in equiaxed solidification of an Al-Cu alloy. It can be said that modeling of coupled columnar and equiaxed solidification with convection has only begun. The purpose of Sec VI is to review the many basic research issues that need to be addressed in modeling of solidification with combined melt convection and solid phase transport.

IV. BASIC MACROSCOPIC MODEL EQUATIONS

This section summarizes the derivations of the macroscopic transport equations. We basically follow the approach taken by other researchers in modeling of a variety of multi-phase systems (Ishii, 1975; Hassanizadeh and Gray, 1979a; Drew, 1983). It is important to note that the present model draws from analyses of both porous-media type systems (e.g., Hassanizadeh and Gray, 1980) and dispersed two-phase flows (e.g., Drew, 1983), in order to cover both columnar and equiaxed growth over the entire range of solid fractions. Traditionally, the literature in these two areas has evolved independently of each other, but in solidification such a division would be artificial. It will soon become apparent that solidification modeling has similar pitfalls to those occurring in other multi-phase models; however, the present approach helps to put the model equations on firmer theoretical grounds and clarifies any assumptions and simplifications made. Besides volume averaging, one could utilize a number of other averaging procedures to derive macroscopic equations (Drew, 1983). The presence of relatively slow moving or stationary, geometrically complex solid structures, however, makes volume averaging particularly appealing from a physical point of view. Most of the following derivations are directly extracted from the above mentioned literature and Ni and Beckermann (1990 and 1991). The equations are simplified as much as possible and the reader is referred to the original literature for a more rigorous and detailed treatment.

IV.1 Volume averaging

The macroscopic conservation equations for each phase are obtained by averaging the microscopic (exact) equations over a volume V_o. This averaging volume must be much smaller than the system and large compared to the characteristic size of the interfacial structures. Each phase k in V_o occupies a volume V_k and is bounded by the interfacial area A_k. The term n_k is the outwardly directed unit normal vector on the interface A_k, and w_k is the velocity of the interface A_k. For completeness, all averaging operators and theorems are given below.

The definition of the volume average of some quantity Ψ in phase k is

$$<\Psi_k> = \frac{1}{V_o} \int_{V_o} X_k \Psi_k dV , \qquad (2)$$

where X_k is a phase function, being equal to unity in phase k and zero otherwise. The intrinsic volume average is defined as

$$<\Psi_k>^k = \frac{1}{V_k} \int_{V_o} X_k \Psi_k dV . \qquad (3)$$

For $\Psi_k=1$, we obtain from Eq (2) the definition of the volume fraction ε_k as

$$\varepsilon_k = V_k/V_o . \qquad (4)$$

In addition, it follows that

$$\sum_k \varepsilon_k = 1 , \qquad (5)$$

and

$$<\Psi_k> = \varepsilon_k <\Psi_k>^k . \qquad (6)$$

The fluctuating component of Ψ_k is defined as

$$\hat{\Psi}_k = (\Psi_k - <\Psi_k>^k) X_k , \qquad (7)$$

and the average of the product of two quantities Ψ_k and Φ_k is given by

$$<\Psi_k \Phi_k>^k = <\Psi_k>^k <\Phi_k>^k + <\hat{\Psi}_k \hat{\Phi}_k>^k . \qquad (8)$$

Finally, we have the following averaging theorems relating the average of a derivative to the derivative of the average (Whitaker, 1967; Slattery, 1967)

$$<\frac{\partial \Psi_k}{\partial t}> = \frac{\partial <\Psi_k>}{\partial t} - \frac{1}{V_o} \int_{A_k} \Psi_k w_k \cdot n_k dA , \qquad (9)$$

$$<\nabla \Psi_k> = \nabla <\Psi_k> + \frac{1}{V_o} \int_{A_k} \Psi_k n_k dA , \qquad (10)$$

and

$$<\nabla \Psi_k> = \varepsilon_k \nabla <\Psi_k>^k + \frac{1}{V_o} \int_{A_k} \hat{\Psi}_k n_k dA . \qquad (11)$$

From a comparison of Eqs (10) and (11), we also obtain

$$\frac{1}{V_o} \int_{A_k} <\Psi_k>^k n_k dA = - <\Psi_k>^k \nabla \varepsilon_k \ , \qquad (12)$$

and for $\Psi_k=1$, we have

$$\frac{1}{V_o} \int_{A_k} n_k \, dA = - \nabla \varepsilon_k \ . \qquad (13)$$

The microscopic (exact) mass, momentum, energy and species conservation equations for a phase k are summarized in Table 1. The energy equation is written in terms of the enthalpy, while the species conservation equation is intended to be representative of each chemical species present. For simplicity, viscous heat dissipation, compression work, as well as volumetric energy and species sources are not included. While this seems appropriate for most practical solidification systems, any of the above assumptions could easily be relaxed.

By integrating the microscopic equations over the averaging volume V_o [and making use of Eqs (2) to (11)], one obtains the corresponding macroscopic equations for phase k and interfacial balances. These equations are also summarized in Table 1. They are valid in every region of the multi-phase system (including the pure solid and liquid regions). Due to the averaging process, integrals over the interfacial area arise in the equations that account for the interactions of phase k with the other phase(s). For simplicity, it is assumed that the correlation between the fluctuating components of ρ_k and Ψ_k, i.e., $<\rho_k \Psi_k>$, is zero, and $<\rho_k>^k$ is simply denoted by ρ_k. Alternatively, one could define density weighted variables (Drew, 1983; Hassanizadeh and Gray, 1979a); however, the resulting form of the equations is virtually identical. In Table 1, the term M_i is the interfacial momentum source due to surface tension. No other interfacial sources are assumed to be present.

IV.2 Basic constitutive relations

The integrals representing the interfacial transfer terms as well as several macroscopic fluxes need to be related to macroscopic (averaged) variables and parameters through so-called constitutive relations. Without making reference to a specific solidification system, one can specify the basic forms of most of these relations, which is demonstrated in this section. All assumptions will be clearly identified. The solid phases are treated as pseudo-fluids.

Surface tension and pressure relations

It has become customary to separate various parts of the interfacial stress M_k^τ given in Table 1 as (Hassanizadeh and Gray, 1979b; Sha et al., 1984)

TABLE 1.   Summary of microscopic and macroscopic monservation equations

Microscopic conservation equations	Macroscopic conservation equations	Interfacial balances	Dispersive fluxes
Mass $\dfrac{\partial \rho_k}{\partial t} + \nabla \cdot (\rho_k v_k) = 0$	$\dfrac{\partial}{\partial t}(\varepsilon_k \rho_k) + \nabla \cdot (\varepsilon_k \rho_k <v_k>^k) = \Gamma_k$	$\sum_k \Gamma_k = 0$	—
Momentum $\dfrac{\partial}{\partial t}(\rho_k v_k) + \nabla \cdot (\rho_k v_k v_k) =$ $-\nabla p_k + \nabla \cdot \tau_k + b_k$	$\dfrac{\partial}{\partial t}(\varepsilon_k \rho_k <v_k>^k) + \nabla \cdot (\varepsilon_k \rho_k <v_k>^k <v_k>^k) =$ $-\nabla(\varepsilon_k <p_k>^k) + \nabla \cdot (<\tau_k> + <\tau_k^t>) + M_k + \varepsilon_k <b_k>^k$	$\sum_k M_k + M_i = 0$	$<\tau_k^t> = - <\rho_k \hat{v}_k \hat{v}_k>$
Energy $\dfrac{\partial}{\partial t}(\rho_k h_k) + \nabla \cdot (\rho_k h_k v_k) =$ $-\nabla \cdot q_k$	$\dfrac{\partial}{\partial t}(\varepsilon_k \rho_k <h_k>^k) + \nabla \cdot (\varepsilon_k \rho_k <h_k>^k <v_k>^k) =$ $-\nabla \cdot (<q_k> + <q_k^t>) + Q_k$	$\sum_k Q_k = 0$	$<q_k^t> = <\rho_k h_k \hat{v}_k>$
Species $\dfrac{\partial}{\partial t}(\rho_k C_k) + \nabla \cdot (\rho_k C_k v_k) =$ $-\nabla \cdot j_k$	$\dfrac{\partial}{\partial t}(\varepsilon_k \rho_k <C_k>^k) + \nabla \cdot (\varepsilon_k \rho_k <C_k>^k <v_k>^k) =$ $-\nabla \cdot (<j_k> + <j_k^t>) + J_k$	$\sum_k J_k = 0$	$<j_k^t> = <\rho_k C_k \hat{v}_k>$

	Total interfacial transfers	Interfacial transfers due to phase change	Interfacial stresses and other transfers
Momentum	$M_k = M_k^\Gamma + M_k^\tau$	$M_k^\Gamma = -\dfrac{1}{V_o} \int_{A_k} \rho_k v_k (v_k - w_k) \cdot n_k \, dA$	$M_k^\tau \dfrac{1}{V_o} \int_{A_k} (\tau_k - p_k I) \cdot n_k \, dA$
Energy	$Q_k = Q_k^\Gamma + Q_k^q$	$Q_k^\Gamma = -\dfrac{1}{V_o} \int_{A_k} \rho_k h_k (v_k - w_k) \cdot n_k \, dA$	$Q_k^q = -\dfrac{1}{V_o} \int_{A_k} q_k \cdot n_k \, dA$
Species	$J_k = J_k^\Gamma + J_k^j$	$J_k^\Gamma = -\dfrac{1}{V_o} \int_{A_k} \rho_k C_k (v_k - w_k) \cdot n_k \, dA$	$J_k^j = -\dfrac{1}{V_o} \int_{A_k} j_k \cdot n_k \, dA$

$$M_k^\tau = \frac{1}{V_o} \int_{A_k} (\tau_k - p_k I)\cdot n_k \, dA$$

$$= +\bar{p}_{ki} \nabla \varepsilon_k + M_k^d , \tag{14}$$

where M_k^d is the dissipative part of the interfacial stress and $\bar{p}_{ki}$ is the average interfacial pressure of phase k. The first term on the right hand side of Eq (14) can be interpreted as a buoyant force due to the average interfacial pressure $\bar{p}_{ki}$. The term M_k^d contains the dissipative interfacial forces due to viscous and form drag and unbalanced pressure distributions leading to lift and virtual mass (acceleration) effects, and is modeled below.

The differences in the interfacial pressures between the phases as well as the interfacial momentum source M_i are due to surface tension. One can show that the two are balanced (Ishii, 1975; Drew, 1983), such that

$$\sum_k \bar{p}_{ki} \nabla \varepsilon_k - M_i = 0 . \tag{15}$$

Substitution of Eqs (14) and (15) into the interfacial momentum balance (see Table 1) yields

$$\sum_k (M_k^\Gamma + M_k^d) = 0 . \tag{16}$$

Next, a relationship between the average interfacial pressure $\bar{p}_{ki}$ and the intrinsic average pressure $<p_k>^k$ needs to be found. Usually, instantaneous microscopic pressure equilibrium in all phases is assumed, which simply yields

$$<p_k>^k = \bar{p}_{ki} . \tag{17}$$

This is a good assumption for the liquid phase(s). If there is significant contact between (equiaxed) crystals or if the solid forms a continuous structure (e.g., in columnar growth), an additional pressure can be transmitted through the solid. At the present time, we assume that the natural state of the solid phase, in the absence of liquid pressure, is stress free. This assumption is often made in porous-media-type flows (Hassanizadeh and Gray, 1980). In dispersed flows, an intergranular stress or contact pressure is sometimes introduced to account for an extra solid pressure (Drew, 1983; Ding and Gidaspow, 1990). This stress is very small before the equiaxed crystals pack and form a (stationary) bed. Since we do not consider stresses and deformations in columnar structures and packings of equiaxed crystals, a solid momentum equation is not needed in regions where a "rigid" solid structure exists. Obviously, this topic needs more attention if one desires to model solid deformations. With Eqs (14) and (17), the macroscopic momentum equation (see Table 1) for all phases can now be written as

$$\frac{\partial}{\partial t}(\varepsilon_k \rho_k <v_k>^k) + \nabla\cdot(\varepsilon_k \rho_k <v_k>^k <v_k>^k)$$

$$= -\varepsilon_k \nabla (<p_k>^k) + \nabla\cdot (<\tau_k> + <\tau_k^t>)$$

$$+ M_k^\Gamma + M_k^d + \varepsilon_k <b_k>^k . \tag{18}$$

Interfacial transfers due to phase change

The exact expressions for the interfacial transfers of mass, momentum, heat, and species due to phase change are provided in Table 1. Physically, these terms represent advection of an interfacial quantity of phase k due to the relative motion of the solid-liquid interface. In view of the mean value theorem for integrals, the terms can be modeled as the product of the interfacial area concentration, A_k/V_o, and a mean interfacial flux. Hence, the interfacial mass transfer rate due to phase change becomes

$$\Gamma_k = A_k/V_o \, \rho_k \bar{w}_{nk} \tag{19}$$

where $\bar{w}_{nk}$ is defined as the average interface velocity of phase k, relative to the velocity of phase k at the interface, normal to the interface and in a direction outward of phase k. In other words, $\bar{w}_{nk}$ represents the normal interface velocity solely due to phase change. The interfacial area concentration A_k/V_o characterizes first-order geometrical effects and is discussed in Sec VI. Similarly, the interfacial momentum, heat, and species transfers due to phase change can be modeled, respectively, as

$$M_k^\Gamma = \bar{v}_{ki} \Gamma_k , \tag{20}$$

$$Q_k^\Gamma = \bar{h}_{ki} \Gamma_k , \tag{21}$$

and

$$J_k^\Gamma = \bar{C}_{ki} \Gamma_k . \tag{22}$$

where the overbar together with the subscript i denote an average over the interfacial area A_k in V_o.

The difference in the interfacial velocities $\bar{v}_{ki}$ between two adjacent phases is solely due to the density difference between the phases. In solidification, the volume change upon phase change is relatively small (as opposed to liquid-vapor or solid-vapor systems), so that the interfacial velocities are about equal. Consequently, the interfacial momentum transfers due to phase change M_k^Γ are approximately balanced and the interfacial momentum balance, Eq (16), reduces to

$$\sum_k M_k^d = 0 \ . \tag{23}$$

It is important to realize that in rapid solidification processes the interfacial momentum transfers due to phase change can be large and will not balance each other. On the other hand, for small Γ_k, M_k^Γ may be neglected completely.

The interfacial enthalpies and concentrations appearing in Eqs (21) and (22) are obtained from thermodynamic relations, which are discussed in Sec IV.3.

Interfacial stress and heat and species transfers

The exact expressions for the interfacial stress M_k^d, heat transfer Q_k^q and species transfer J_k^j are given by Eq (14) and in Table 1. Physically, these terms represent the transport phenomena between the phases within V_o by convection and/or diffusion. The interfacial transfers are due to microscopic velocity, temperature, and species concentration gradients on each side of the solid-liquid interface A_k. Similarly to the interfacial transfers due to phase change, they can generally be modeled as the product of the interfacial area concentration A_k/V_O and a mean interfacial flux. It can be assumed that the mean interfacial flux is, in turn, directly proportional to the difference between the interfacial average and the intrinsic volume average of a quantity of phase k, i.e., $\overline{\Psi}_{ki} - <\Psi_k>^k$. In other words, the difference $\overline{\Psi}_{ki} - <\Psi_k>^k$ is assumed to be the *driving force* for the interfacial fluxes. Mathematically, this can be expressed as

$$M_k^d = (\frac{A_k}{V_o}) \, R_k \, (\overline{v}_{ki} - <v_k>^k) \ , \tag{24}$$

$$Q_k^q = (\frac{A_k}{V_o}) \frac{k_k}{\ell_k^q} (\overline{T}_{ki} - <T_k>^k)$$

$$= (\frac{A_k}{V_o}) \, h_k \, (\overline{T}_{ki} - <T_k>^k) \ , \tag{25}$$

and

$$J_k^j = (\frac{A_k}{V_o}) \, \rho_k \frac{D_k}{\ell_k^j} (\overline{C}_{ki} - <C_k>^k)$$

$$= (\frac{A_k}{V_o}) \, \rho_k \, h_{mk} \, (\overline{C}_{ki} - <C_k>^k) \ , \tag{26}$$

where R_k is a resistance coefficient and h and h_m are average convective heat and mass transfer coefficients, respectively. The meanings of the various diffusion lengths, ℓ, are illustrated in Fig 6. The region shown in Fig 6 represents an infinitesimally small section of the interfaces depicted in Fig

3 and is drawn, for simplicity, as a straight line. In general, these lengths (or the heat and mass transfer coefficients) and R_k are complicated functions of the solid microstructure, volume fractions, interface velocities and curvatures, time, heat and mass transfer, and melt flow conditions in the averaging volume. Although Eqs (24) to (26) are not directly usable at this point, we have succeeded in expressing the interfacial transfers in terms of macroscopic variables and parameters. The coefficients (and A_k/V_o) must generally be obtained from microscopic models and experimental measurements, which is discussed in Secs V and VI.

Macroscopic shear stresses and heat and species fluxes

The viscous stress $<\tau_k>$, heat flux $<q_k>$, and species flux $<j_k>$ represent interactions *within* a phase (i.e., of a phase with itself). Constitutive relations for these macroscopic fluxes can be obtained under the following simplifying assumptions:

(1) The viscous stresses are proportional to the rates of deformation. The contribution to the viscous stresses due to displacement gradients (arising from density differences and phase change) are negligibly small (Drew, 1983). The solid phase is viewed as a pseudo-fluid (see Sec VI.2 for a discussion).
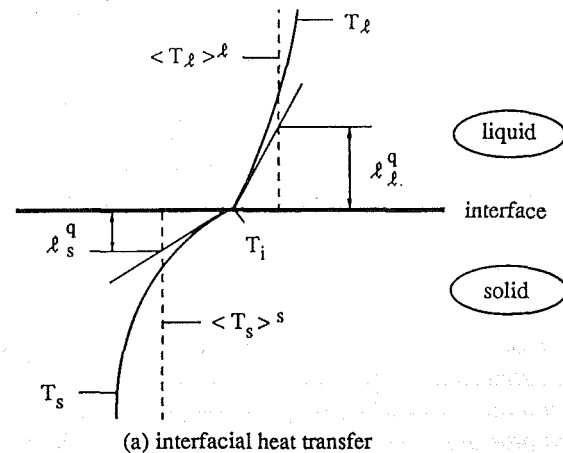
(a) interfacial heat transfer
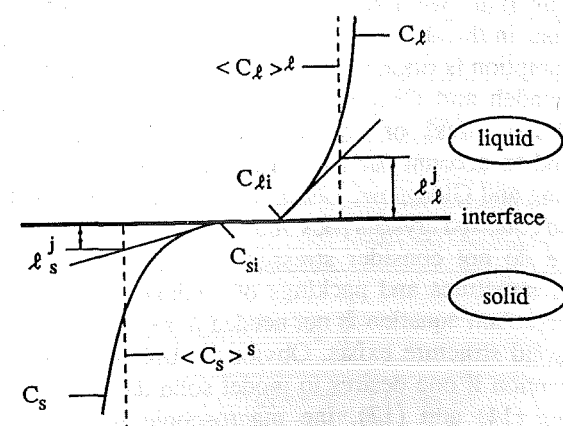
(b) interfacial species transfer

FIG 6.   Illustration of the diffusion lengths: (a) interfacial heat transfer and (b) interfacial species transfer (Ni and Beckermann, 1990).

(2) The microscopic heat and species diffusion fluxes are given by Fourier's and Fick's laws, respectively. Other diffusional fluxes (e.g., the Soret and Dufour effects, Bird et al., 1960) are usually not important in conventional solidification processes (Poirier et al., 1991).

(3) The fluctuating components of the viscosity, thermal conductivity, and species diffusion coefficient of phase k are negligibly small. This assumption is generally invoked in volume averaging (Hassanizadeh and Gray, 1979a and 1979b), but its accuracy has not been established. In solidification, it can be expected to be good because of small variations of these thermophysical properties on a microscopic scale.

The following relations can now be written,

$$<\tau_k> = \mu_k <\nabla v_k + (\nabla v_k)^t> , \tag{27}$$

$$<q_k> = - k_k \cdot <\nabla T_k> , \tag{28}$$

and

$$<j_k> = - D_k \cdot \rho_k <\nabla C_k> . \tag{29}$$

Using the averaging theorems given by Eqs (10) and (11), the above equations can be rewritten as

$$<\tau_k> = \mu_k \{ \nabla (\varepsilon_k <v_k>^k) + [\nabla (\varepsilon_k <v_k>^k)]^t$$

$$+ \frac{1}{V_o} \int_{A_k} v_k \, n_k \, dA + \frac{1}{V_o} \int_{A_k} n_k \, v_k \, dA \} , \tag{30}$$

$$<q_k> = - k_k \cdot [\varepsilon_k \nabla <T_k>^k + \frac{1}{V_o} \int_{A_k} \hat{T}_k \, n_k \, dA] , \tag{31}$$

and

$$<j_k> = - D_k \cdot \rho_k [\varepsilon_k \nabla <C_k>^k + \frac{1}{V_o} \int_{A_k} \hat{C}_k \, n_k \, dA] . \tag{32}$$

Again, the integrals appearing in Eqs (30) to (32) need to be related to macroscopic variables. In view of the averaging theorem given by Eq (12), Eq (30) may be expressed as

$$<\tau_k> = \mu_k^* \{ \nabla (\varepsilon_k <v_k>^k) + [\nabla (\varepsilon_k <v_k>^k)]^t$$

$$- \bar{v}_{ki} (\nabla \varepsilon)_k - (\nabla \varepsilon_k) \bar{v}_{ki} \} , \tag{33}$$

where μ_k^* is an effective viscosity. A similar model has been proposed by Ishii (1975). The integrals in Eqs (31) and (32) are typically modeled by introducing (stagnant) effective thermal conductivities and mass diffusivities as

$$<q_k> = - k_k^* \cdot \varepsilon_k \nabla <T_k>^k \tag{34}$$

and

$$<j_k> = - D_k^* \cdot \rho_k \varepsilon_k \nabla <C_k>^k . \tag{35}$$

The material coefficients μ_k^*, k_k^* and D_k^* are generally different from their microscopic counterparts and depend, for example, on the microstructure. This is discussed in more detail in Secs V and VI.

One also needs to model the macroscopic *dispersive* stresses, heat and species fluxes given in Table 1. Traditionally, this has been accomplished through the use of increased viscosities, thermal conductivities, and mass diffusivities. For multi-phase flows, this is an area of considerable research and controversy. Only models of limited validity are available and it is not clear how the dispersive fluxes can be modeled in solidification systems. It is, however, important to realize that the dispersive fluxes in the pure liquid region are non-zero if the flow is turbulent.

IV.3 Thermodynamic relations

Interfacial temperatures and concentrations

Under the assumption of thermodynamic equilibrium, the temperatures of the phases at any point on an interface are the same, so that we can write

$$T_{ki} = T_i . \tag{36}$$

This temperature is, in turn, related to the interfacial species concentrations through the equilibrium phase diagram, i.e.,

$$C_{ki} = g(T_i) , \tag{37}$$

where g_k is, for example, the equation describing the liquidus or solidus lines. The above equations can be modified to account for deviations from the phase diagram due to kinetic, curvature, or pressure effects (Flemings, 1974; Kurz and Fisher, 1989).

The above *local* conditions need to be related to the *average interfacial* temperatures and concentrations for use in the interfacial balances. For this purpose, T_{ki} and C_{ki} are regarded as simple (i.e., non-weighted) averages over the interfaces in the averaging volume. Then, we can write immediately

$$\bar{T}_{ki} = \bar{T}_i . \tag{38}$$

However, Eq (37) holds on an average basis only if T_i is uniform on A_k, because the function g_k may be nonlinear. An isothermal interface is usually a good assumption for dendrite tips (Kurz and Fisher, 1989). However, for strongly varying interfacial curvatures and/or for highly directional heat and species fluxes at the interface (which may be caused by convection), T_i will be nonuniform. This problem can be overcome by linearizing the function g_k so that

$$\bar{C}_{ki} = g_k^{\ell}(\bar{T}_i),\tag{39}$$

where the superscript ℓ indicates a linearized phase diagram. Note that Eqs (38) and (39) are generally not valid for the volume averaged temperatures and concentrations, $<T_k>^k$ and $<C_k>^k$.

Enthalpies and densities

Neglecting the influence of pressure, the local enthalpy and density of phase k can be obtained from appropriate state functions, i.e.,

$$h_k = h_k(T_k, C_k)\tag{40}$$

and

$$\rho_k = \rho_k(T_k, C_k),\tag{41}$$

where C_k stands for the concentration of each species present. Again, Eqs (40) and (41) are *local* conditions that need to be expressed in terms of *average* quantities for use in the macroscopic equations. Unless the microscopic temperature and concentration profiles in the averaging volume are known (e.g., if they are uniform), the state functions need to be linearized in both temperature and species concentration. Note that this is equivalent to introducing constant specific heats and coefficients of expansion. Then,

$$<h_k>^k = \frac{1}{V_k}\int_{V_o} X_k h_k(T_k, C_k)dV$$

$$= h_k^{\ell}(<T_k>^k, <C_k>^k),\tag{42}$$

$$<\rho_k>^k = \frac{1}{V_k}\int_{V_o} X_k \rho_k(T_k, C_k)dV$$

$$= \rho_k^{\ell}(<T_k>^k, <C_k>^k),\tag{43}$$

and also

$$\bar{h}_{ki} = h_k^{\ell}(\bar{T}_{ki}, \bar{C}_{ki}),\tag{44}$$

$$\bar{\rho}_{ki} = \rho_k^{\ell}(\bar{T}_{ki}, \bar{C}_{ki}),\tag{45}$$

where the superscript ℓ indicates that these functions are linearized in all variables. Also note that the difference between the *interfacial* liquid and solid enthalpies, but not the volume averaged ones, is equal to the latent heat of fusion, unless the temperatures and concentrations in both phases are uniform.

V. A MODEL FOR COLUMNAR SOLIDIFICATION

In this section, a macroscopic model is reviewed that is limited to columnar solidification, with the solid rigid and fixed to a cooled wall. In addition, a number of other simplifying assumptions with regard to processes on a microscopic scale are made to reduce the equations to forms that can theoretically be solved; these are discussed below. Nevertheless, several challenging modeling issues remain that need research attention. The model (Schneider, 1991) is basically a generalized version of the models used by Bennon and Incropera (1987), Beckermann and Viskanta (1988), Voller et al. (1989) and others to predict convection and macrosegregation during columnar solidification of binary alloys. The approach taken is the same as the one exemplified by Eq (1), except that liquid convection is included. We consider a binary alloy with a phase diagram corresponding to the one shown in Fig 2. The phase diagram reveals that at most three phases are present during solidification: liquid ($k=\ell$), α-phase solid ($k=\alpha$), and β-phase solid ($k=\beta$). The main assumptions can be summarized as follows:

(1) The solid phases are rigid and stationary (as in purely columnar growth) so that $v_\alpha = v_\beta = 0$.

(2) All phases in the averaging volume are in thermal equilibrium so that $<T_\ell>^\ell = <T_\alpha>^\alpha = <T_\beta>^\beta = \bar{T}_{\ell i} = \bar{T}_{\alpha i} = \bar{T}_{\beta i} = \bar{T}_i = T$. This assumption can be justified by the high thermal diffusivity of metal alloys and the presence of creeping flow in the columnar mushy zone. Its validity is also discussed in connection with Eq (1).

(3) The liquid in the averaging volume is solutally well mixed so that $<C_\ell>^\ell = \bar{C}_{\ell i}$. This is typically a good assumption for the liquid within the interdendritic meshwork, but produces errors at the dendrite tips due to solutal undercooling (Flood and Hunt, 1987; Huppert, 1990). The main drawback of this assumption is that a kinetic law for the movement of the dendrite tips cannot be included (Rappaz, 1989).

(4) Species diffusion in the solid phases (α and β) within the averaging volume is either complete (so that $<C_\alpha>^\alpha = \bar{C}_{\alpha i}$ and $<C_\beta>^\beta = \bar{C}_{\beta i}$) or absent (i.e., $D_\alpha = D_\beta = 0$). This assumption basically covers two important limiting cases as discussed below.

(5) All dispersion fluxes are neglected. Therefore, the model is limited to creeping flow in the mushy zone and laminar flow in the pure liquid region. The important effects of turbulent melt flow cannot be addressed with such a model.

Note that modeling of equiaxed solidification would be meaningless with this model, because of the neglect of undercooling of the liquid (and, of course, the assumption of a stationary solid).

V.1 Conservation equations

In order to avoid modeling of the interfacial transfer terms, the conservation equations for each phase can be added up to obtain the so-called mixture equations, where terms accounting for the interfacial transfers have cancelled out due to the interfacial balance requirements. The liquid momentum equation needs to be considered separately, because we want to account for interfacial momentum transfer due to friction of the liquid in the mushy zone. Similarly, the solid mass and species conservation equations are considered separately, because of assumption (4). In the following, useful forms of the various conservation equations are developed. All equations are taken directly from Sec IV.

Mass conservation

By adding up the phase mass conservation equations given in Table 1, and making use of the interfacial mass balance, we obtain the mixture mass conservation equation

$$\frac{\partial}{\partial t}(\varepsilon_\ell \rho_\ell) + \nabla \cdot (\varepsilon_\ell \rho_\ell <v_\ell>^\ell) = -\frac{\partial}{\partial t}(\varepsilon_\alpha \rho_\alpha + \varepsilon_\beta \rho_\beta) \ .$$

(46)

In addition the individual mass conservation equations for the solid phases, i.e.,

$$\frac{\partial}{\partial t}(\varepsilon_\alpha \rho_\alpha) = \Gamma_\alpha$$

(47)

and

$$\frac{\partial}{\partial t}(\varepsilon_\beta \rho_\beta) = \Gamma_\beta$$

(48)

will be needed in the derivation of the solid species conservation equations.

Species (solute) conservation

The mixture species equation is given by

$$\frac{\partial}{\partial t}(\varepsilon_\ell \rho_\ell <C_\ell>^\ell + \varepsilon_\alpha \rho_\alpha <C_\alpha>^\alpha + \varepsilon_\beta \rho_\beta <C_\beta>^\beta)$$

$$+ \nabla \cdot (\varepsilon_\ell \rho_\ell <C_\ell>^\ell <v_\ell>^\ell)$$

$$= -\nabla \cdot (<j_\ell> + <j_\alpha> + <j_\beta>)$$

(49)

Due to the small mass diffusivity of solid alloys, we can safely assume that $<j_\alpha>=<j_\beta>=0$. Note that this assumption does not rule out the possibility of species diffusion in the solid on a microscopic scale, i.e., within the averaging volume. The macroscopic species diffusion flux in the liquid is given by Eq (35) with $k=\ell$. The inclusion of finite rate macroscopic species diffusion in the liquid, $<j_\ell>$, is important for the prediction of double-diffusive convection phenomena (see Sec II), and does not preclude the assumption of a solutally well-mixed liquid on a microscopic scale. In addition, we will assume, for simplicity, that $D^*_\ell = D_\ell$. Because Eq (49) is used to calculate the liquid concentration, it is expanded and written as

$$\varepsilon_\ell \rho_\ell \frac{\partial <C_\ell>^\ell}{\partial t} + \varepsilon_\ell \rho_\ell <v_\ell>^\ell \cdot \nabla <C_\ell>^\ell$$

$$= \nabla \cdot (\varepsilon_\ell \rho_\ell D_\ell \nabla <C_\ell>^\ell) - \varepsilon_\alpha \rho_\alpha \frac{\partial <C_\alpha>^\alpha}{\partial t}$$

$$- \varepsilon_\beta \rho_\beta \frac{\partial <C_\beta>^\beta}{\partial t} + (<C_\ell>^\ell - <C_\alpha>^\alpha)\frac{\partial}{\partial t}(\varepsilon_\alpha \rho_\alpha)$$

$$+ (<C_\ell>^\ell - <C_\beta>^\beta)\frac{\partial}{\partial t}(\varepsilon_\beta \rho_\beta) \ .$$

(50)

The last two terms on the right hand side of Eq (50) represent sources of species upon solidification due to the different compositions of the solid and liquid phases. Note that the concentration differences in these terms are volume averaged and not interfacial concentrations. Equation (50) could equally well be derived by starting from the liquid species concentration equation [instead of Eq (49)], and eliminating the interfacial transfer terms by substitution from the interfacial species balance and the solid species conservation equations (see Table 1). From this point of view, Eq (50) can also be regarded as a *liquid*, instead of a mixture, species conservation equation. The same can be said of the mass conservation equation, Eq (46).

Assuming negligible macroscopic species diffusion fluxes in the solid and utilizing Eqs (22), (26), (47), and (48), the solid species conservation equations for the two solid phases become

$$\varepsilon_\alpha \rho_\alpha \frac{\partial <C_\alpha>^\alpha}{\partial t}$$

$$= (\bar{C}_{\alpha i} - <C_\alpha>^\alpha) \ [\frac{\partial}{\partial t}(\varepsilon_\alpha \rho_\alpha) + (\frac{A_\alpha}{V_o})\frac{\rho_\alpha D_\alpha}{\ell_\alpha^j}]$$

(51)

and

$$\varepsilon_\beta \rho_\beta \frac{\partial <C_\beta>^\beta}{\partial t}$$

$$= (\overline{C}_{\beta i} - <C_\beta>^\beta) \left[\frac{\partial}{\partial t} (\varepsilon_\beta \rho_\beta) + \left(\frac{A_\beta}{V_o} \right) \frac{\rho_\beta D_\beta}{\mathscr{l}_\beta^j} \right] . \qquad (52)$$

The above two equations allow for the calculation of the average solid concentrations as a function of the interfacial values, provided the last terms on the right hand sides can be related to known parameters. For simplicity, we will consider two limiting cases, i.e.,

$$\left(\frac{A_\alpha}{V_o} \right) \frac{\rho_\alpha D_\alpha}{\mathscr{l}_\alpha^j} \rightarrow \infty , \qquad \left(\frac{A_\beta}{V_o} \right) \frac{\rho_\beta D_\beta}{\mathscr{l}_\beta^j} \rightarrow \infty , \qquad (53)$$

and

$$\left(\frac{A_\alpha}{V_o} \right) \frac{\rho_\alpha D_\alpha}{\mathscr{l}_\alpha^j} = 0 , \qquad \left(\frac{A_\beta}{V_o} \right) \frac{\rho_\beta D_\beta}{\mathscr{l}_\beta^j} = 0 . \qquad (54)$$

The first case, Eq (53), is approached for a very finely dispersed solid microstructure, where the interfacial area concentrations are large (and, hence, the diffusion lengths are small). Substitution of Eq (53) into Eqs (51) and (52) will force the average solid concentrations to be equal to the corresponding interfacial values, implying solutally well mixed solid phases on a microscopic scale. The second case, Eq (54), is true for negligibly small solid mass diffusivities and microstructures that have a small surface area to volume ratio. Then, the solid will have "layers" of different composition that reflect the interfacial concentrations at various instants of time during solidification. The above two cases have been known to metallurgists for many years (see Flemings, 1974), but volume averaging provides a clear understanding of the parameters involved. A model with *finite* rate solid diffusion on a microscopic scale is presented in Sec VI. A different one has been developed by Poirier et al. (1991). Whether Eq (53) or (54) is more realistic depends on the alloy and the solidification conditions. For example, in the Fe-C system the solid mass diffusivities are relatively large and Eq (53) is generally a better approximation. For diffusion-dominated solidification of a Pb-Sn alloy it has been found that predictions of the liquidus isotherm positions differ by less than 3% between the two limiting cases (Schneider and Beckermann, 1991). However, the local solid fractions and the volume of eutectic phase in the final solid (an important metallurgical parameter) can be quite different, depending on the initial concentrations (Poirier et al., 1991). Voller et al. (1989) found for solidification of a NH4Cl-H2O solution with convection that the predictions are quite similar; however, this probably needs more investigation for metal alloys.

The presence of a microscopic concentration profile in the solid phase for the model specified in Eq (54) causes special problems during remelting of solid (Rappaz and Voller, 1990; Poirier et al., 1991). Remelting can occur due to advection of liquid of different temperature and composition in the mushy zone or due to solutal layering in the pure liquid region (Beckermann and Viskanta, 1988). The changes in the average solid concentration during remelting depend on the (microscopic) concentration profile "frozen" in the solid at earlier times. One method to handle remelting would be to record the microscopic concentration profile by "remembering" the interfacial solid concentrations at all times. During remelting one would simply back up along this record. However, this recording process would be an extremely time and space consuming task. In addition, it may be argued that remelting is not the exact reverse of solidification, because various parts of the solid can remelt at different rates. One way of circumventing this problem may be to assume that the solid that melts has a composition equal to the *average* solid concentration before remelting, i.e., $<C_\alpha>^\alpha$, $<C_\beta>^\beta$=constant during remelting (Schneider, 1991). This statement can readily be incorporated into the solution of Eqs (51) and (52) together with Eq (54). More realistic modeling of remelting in the presence of microscopic solute profiles in the solid would first require careful experimentation. Since the solid is assumed to be solutally well mixed on a microscopic scale when using Eq (53), no such problem exists during modeling of remelting.

Energy conservation

The mixture energy equation is given by

$$\frac{\partial}{\partial t} (\varepsilon_\mathscr{l} \rho_\mathscr{l} <h_\mathscr{l}>^\mathscr{l} + \varepsilon_\alpha \rho_\alpha <h_\alpha>^\alpha + \varepsilon_\beta \rho_\beta <h_\beta>^\beta +$$

$$+ \nabla \cdot (\varepsilon_\mathscr{l} \rho_\mathscr{l} <h_\mathscr{l}>^\mathscr{l} <v_\mathscr{l}>^\mathscr{l})$$

$$= - \nabla \cdot (<q_\mathscr{l}> + <q_\alpha> + <q_\beta>) . \qquad (55)$$

Because of assumption (2) and in analogy with Eq (1), it is of advantage to use the temperature T as the dependent variable in Eq (55) [however, this is not necessary as shown by Bennon and Incropera (1987)]. Assuming an equation of the form of Eq (42) can be specified, the differential of the average enthalpy of a phase is

$$d<h_k>^k = \left. \frac{\partial <h_k>^k}{\partial T} \right|_{<C_k>^k} dT + \left. \frac{\partial <h_k>^k}{\partial <C_k>^k} \right|_T d<C_k>^k .$$
$$(56)$$

Substituting Eqs (34) and (56) into Eq (55), yields after a few steps

$$\left[\left. \varepsilon_\mathscr{l} \rho_\mathscr{l} \frac{\partial <h_\mathscr{l}>^\mathscr{l}}{\partial T} \right|_{<C_\mathscr{l}>^\mathscr{l}} + \left. \varepsilon_\alpha \rho_\alpha \frac{\partial <h_\alpha>^\alpha}{\partial T} \right|_{<C_\alpha>^\alpha}$$

$$+ \; \varepsilon_\beta \rho_\beta \frac{\partial <h_\beta>^\beta}{\partial T} \Bigg|_{<C_\beta>^\beta} \;] \; \frac{\partial T}{\partial t}$$

$$+ \; \varepsilon_\ell \rho_\ell \frac{\partial <h_\ell>^\ell}{\partial T} \Bigg|_{<C_\ell>^\ell} \; <v_\ell>^\ell \cdot \nabla T$$

$$+ \; \varepsilon_\ell \rho_\ell \frac{\partial <h_\ell>^\ell}{\partial <C_\ell>^\ell} \Bigg|_{T} \; \frac{\partial <C_\ell>^\ell}{\partial t}$$

$$+ \; \varepsilon_\alpha \rho_\alpha \frac{\partial <h_\alpha>^\alpha}{\partial <C_\alpha>^\alpha} \Bigg|_{T} \; \frac{\partial <C_\alpha>^\alpha}{\partial t}$$

$$+ \; \varepsilon_\beta \rho_\beta \frac{\partial <h_\beta>^\beta}{\partial <C_\beta>^\beta} \Bigg|_{T} \; \frac{\partial <C_\beta>^\beta}{\partial t})$$

$$+ \; \varepsilon_\ell \rho_\ell \frac{\partial <h_\ell>^\ell}{\partial <C_\ell>^\ell} \Bigg|_{T} \; <v_\ell>^\ell \cdot \nabla <C_\ell>^\ell$$

$$= \nabla \cdot \left[(\varepsilon_\ell k_\ell^* + \varepsilon_\alpha k_\alpha^* + \varepsilon_\beta k_\beta^*) \nabla T \right]$$

$$+ \; [<h_\ell>^\ell - <h_\alpha>^\alpha] \frac{\partial (\varepsilon_\alpha \rho_\alpha)}{\partial t}$$

$$+ \; [<h_\ell>^\ell - <h_\beta>^\beta] \frac{\partial (\varepsilon_\beta \rho_\beta)}{\partial t} \; . \tag{57}$$

Note that the interdiffusive and Dufour heat fluxes (Bird et al., 1960) have been neglected in the first terms on the the right-hand-side of Eq (57), since the Lewis number of metal alloys is very large ($\sim 10^4$). The volume fraction weighted sum of the effective phase thermal conductivities can be termed a "mixture" thermal conductivity. Its value depends on the microstructure. While many theoretical and empirical formulae for the mixture thermal conductivity are available for porous-media type systems, it is not clear how it can be calculated for the wide variety of microstructures present in the system considered here. It would be useful to conduct experiments to directly measure the mixture thermal conductivity as a function of the volume fractions; however, no such data has yet been reported in the literature. Due to the directional nature of columnar dendritic structures, one would expect the effective thermal conductivity to be anisotropic. As a first approximation, the effective phase thermal conductivities may be taken equal to their microscopic counterparts, i.e., $k_k^* = k_k$. In addition, it should be mentioned that very little data is available for the temperature *and* concentration dependencies of the phase thermal conductivities of practical metal alloys. The above discussion also applies to the mass diffusivities. Note that the differences in the average solid and liquid enthalpies

appearing in the last two terms on the right-hand-side of Eq (57) are generally not equal to the latent heats of fusion, unless all phases are solutally (and thermally) well mixed within V_O (see Sec IV.3). The latent heat of fusion of the α-phase and β-phase solids can be quite different (Poirier and Nandapurkar, 1988).

In a numerical solution, the last term on the left-hand-side of Eq (57) would require a relatively complicated discretization procedure (Patankar, 1982). On the other hand, time derivatives are much easier to discretize than advective terms. The advective term involving the liquid concentration can be eliminated by solving the mixture species conservation equation, Eq (50), for this term, multiplying it by $(\partial <h_\ell>^\ell / \partial <C_\ell>^\ell)_T$, and substituting it into Eq (57). All macroscopic species diffusion terms can, again, be safely neglected in the energy equation. The result is

$$\left[\; \varepsilon_\ell \rho_\ell \frac{\partial <h_\ell>^\ell}{\partial T} \Bigg|_{<C_\ell>^\ell} + \varepsilon_\alpha \rho_\alpha \frac{\partial <h_\alpha>^\alpha}{\partial T} \Bigg|_{<C_\alpha>^\alpha} \right.$$

$$\left. + \; \varepsilon_\beta \rho_\beta \frac{\partial <h_\beta>^\beta}{\partial T} \Bigg|_{<C_\beta>^\beta} \; \right] \; \frac{\partial T}{\partial t}$$

$$+ \; \varepsilon_\ell \rho_\ell \frac{\partial <h_\ell>^\ell}{\partial T} \Bigg|_{<C_\ell>^\ell} \; <v_\ell>^\ell \cdot \nabla T$$

$$= \nabla \cdot \left[(\varepsilon_\ell k_\ell^* + \varepsilon_\alpha k_\alpha^* + \varepsilon_\beta k_\beta^*) \nabla T \right]$$

$$- \; \varepsilon_\ell \rho_\ell \frac{\partial <h_\ell>^\ell}{\partial <C_\ell>^\ell} \Bigg|_{T} \; \frac{\partial <C_\ell>^\ell}{\partial t}$$

$$- \; \varepsilon_\alpha \rho_\alpha \frac{\partial <h_\alpha>^\alpha}{\partial <C_\alpha>^\alpha} \Bigg|_{T} \; \frac{\partial <C_\alpha>^\alpha}{\partial t}$$

$$- \; \varepsilon_\beta \rho_\beta \frac{\partial <h_\beta>^\beta}{\partial <C_\beta>^\beta} \Bigg|_{T} \; \frac{\partial <C_\beta>^\beta}{\partial t})$$

$$+ \; \frac{\partial <h_\ell>^\ell}{\partial <C_\ell>^\ell} \Bigg|_{T} \; \{ \; \varepsilon_\ell \rho_\ell \frac{\partial <C_\ell>^\ell}{\partial t} + \varepsilon_\alpha \rho_\alpha \frac{\partial <C_\alpha>^\alpha}{\partial t}$$

$$+ \; \varepsilon_\beta \rho_\beta \frac{\partial <C_\beta>^\beta}{\partial t} - (<C_\ell>^\ell - <C_\alpha>^\alpha) \frac{\partial}{\partial t} (\varepsilon_\alpha \rho_\alpha)$$

$$- \; (<C_\ell>^\ell - <C_\beta>^\beta) \frac{\partial}{\partial t} (\varepsilon_\beta \rho_\beta) \; \}$$

$$+ \; [<h_\ell>^\ell - <h_\alpha>^\alpha] \frac{\partial (\varepsilon_\alpha \rho_\alpha)}{\partial t}$$

$$+ [<h_\ell>^\ell - <h_\beta>^\beta] \frac{\partial(\varepsilon_\beta \rho_\beta)}{\partial t} . \tag{58}$$

Although lengthy, Eq (58) can easily be discretized using standard numerical discretization procedures (e.g, Patankar, 1982). In addition, Eq (58) is written in a form that is consistent with the mass [Eq (46)] and species [Eq (50)] conservation equations. Special care should be taken to discretize the unsteady terms involving $(\partial T/\partial t)$ consistently so that Eq (58) can be solved for the temperature in all regions of the domain (i.e., solid, liquid and mush) (see also Sec V.2).

Momentum conservation

For a stationary and rigid solid phase and neglecting the interfacial momentum transfer due to density changes upon phase-change (i.e.,$\bar{v}_{\ell i} \approx \bar{v}_{si} = 0$), the liquid momentum equation, Eq (18), becomes

$$\frac{\partial}{\partial t}(\varepsilon_\ell \rho_\ell <v_\ell>^\ell) + \nabla\cdot(\varepsilon_\ell \rho_\ell <v_\ell>^\ell <v_\ell>^\ell)$$

$$= - \varepsilon_\ell \nabla<p_\ell>^\ell$$

$$+ \nabla\cdot \{ \mu_\ell^* [\nabla(\varepsilon_\ell<v_\ell>^\ell) + (\nabla(\varepsilon_\ell <v_\ell>^\ell))^t] \}$$

$$- (A_\ell/V_o) R_\ell <v_\ell>^\ell + \varepsilon_\ell \rho_\ell g \tag{59}$$

where (i) Eq (24) (with $\bar{v}_{\ell i}=0$) has been substituted for the interfacial drag term M_ℓ^d, (ii) Eq (33) (with $\bar{v}_{\ell i}=0$) has been substituted for the macroscopic shear stress, and (iii) the body force has been assumed to be due to gravity only. Equation (59) can be written in the same form as the species and energy conservation equations by expanding various terms and utilizing the continuity equation. Generally, one has the choice of choosing the volume averaged (or "superficial") velocity $<v_\ell>=\varepsilon_\ell<v_\ell>^\ell$ or the intrinsic volume averaged (or "pore") velocity $<v_\ell>^\ell$ as the dependent variable (Voller et al., 1989). The choice depends on the numerical discretization procedure to be used, but the overall discretization effort is approximately the same (Schneider, 1991). Here, we choose the pore velocity $<v_\ell>^\ell$ as the dependent variable and rewrite Eq (59) as

$$\varepsilon_\ell \rho_\ell \frac{\partial<v_\ell>^\ell}{\partial t} + \varepsilon_\ell \rho_\ell <v_\ell>^\ell \cdot \nabla<v_\ell>^\ell$$

$$= - \varepsilon_\ell \nabla<p_\ell>^\ell$$

$$+ \nabla\cdot \{ \varepsilon_\ell \mu_\ell^* [\nabla<v_\ell>^\ell + (\nabla<v_\ell>^\ell)^t]$$

$$+ \mu_\ell^* [<v_\ell>^\ell \nabla\varepsilon_\ell + \nabla\varepsilon_\ell<v_\ell>^\ell] \}$$

$$+ <v_\ell>^\ell [\frac{\partial}{\partial t}(\varepsilon_\alpha \rho_\alpha + \varepsilon_\beta \rho_\beta)]$$

$$- (A_\ell/V_o) R_\ell <v_\ell>^\ell + \varepsilon_\ell \rho_\ell g \tag{60}$$

The effective liquid viscosity μ_ℓ^* is often taken to be equal to the actual liquid viscosity (Neale and Nader, 1974; Ganesan and Poirier, 1990; Prescott et al., 1991). However, it is well known in the porous media literature that μ_ℓ^* depends on the solid structure (e.g., Lundgren, 1972). This can be visualized by considering the extreme case of the liquid being contained in small pockets formed by the dendritic meshwork. No shear stress can be transferred by such a liquid on a macroscopic scale, so that μ_ℓ^* should vanish. Accurate specification of μ_ℓ^* is also important near the mush/liquid interface (i.e., for $\varepsilon_\ell \to 1$), where velocity gradients can be large (Larson and Higdon, 1986; Sahraoui and Kaviany, 1991). Due to the absence of a general theory or experimental measurements for columnar dendrites, one has little choice but to take $\mu_\ell^*=\mu_\ell$.

The main problem with Eq (60) is the complete specification of the interfacial drag in terms of known parameters. This requires consideration of the flow on a microscopic scale. The directional nature of the columnar dendritic structure causes the resistance coefficient R_ℓ to be anisotropic. Poirier (1987) recently discussed a variety of models for interdendritic flow in columnar alloys. Typically, the mushy zone is viewed as porous medium and the resistance coefficient R_ℓ is identified with a permeability. This can be written as

$$M_\ell^d = - (A_\ell/V_o) R_\ell <v_\ell>^\ell = - \varepsilon_\ell^2 \mu_\ell K^{(2)^{-1}} <v_\ell>^\ell \tag{61}$$

where $K^{(2)}$ is a symmetric permeability tensor. The permeability contains the interfacial area concentration implicitly. Models for the permeability can rigorously be derived by considering laminar, fully developed flow through capillary fissures or tube bundles (Bird et al., 1960). Accordingly, a component of the permeability is given by

$$K = \frac{\varepsilon_\ell^3}{C_k(A_\ell/V_o)^2} \tag{62}$$

where C_k (≈ 5) is sometimes called Kozeny's constant. The interfacial area concentration A_ℓ/V_o can, in turn, be related to a hydraulic radius, r_h, through

$$A_\ell/V_o = \varepsilon_\ell/r_h \tag{63}$$

and r_h may be related to the primary and secondary dendrite arm spacings (Poirier, 1987). Although models of the above form provide insight into the basic dependencies of the permeability, they still need "calibration" through experiments (see Poirier, 1987 and references therein for a

compilation of such measurements). While numerous data are available for small and intermediate liquid fractions, no measurements of the permeability have been reported for liquid fractions approaching unity. This represents a serious deficiency, because the flow in the dendrite tip region can be expected to have a crucial influence on the growth of microstructures and the transport of heat and species by convection. A modification to the above permeability model for high liquid fractions is discussed in Sec VI.1. Ganesan et al. (1992) recently presented a study of the permeability parallel to the primary dendrite arms for solid fractions below 0.35, for which there are no experimental data available. In a promising approach, they combined descriptions of real microstructures taken from quenched solidification experiments with direct numerical simulations of the microscopic flow. The effect of anisotropy in the permeability of the mushy region during solidification of a binary mixture (NH_4Cl-H_2O) was examined numerically by introducing the principal permeability ratio R (Yoo and Viskanta, 1992). A small R was found to promote not only the growth of the secondary layer but also result in a large concentration difference between the mushy and the pure liquid region. Also, severe remelting was found to occur due to the liquidus temperature depression by higher concentration and the earlier development of thermal convection in the upper layer.

An area where accurate permeability data is of particular importance is in the prediction of channel segregates in castings. Several studies have recently been reported where the formation of channel segregates has been simulated (Prescott and Incropera, 1991; Felicelli et al., 1991). The evolution of the permeability in such channels should be the subject of more investigation, particularly because the dendritic structure in the channels can be expected to be quite different from that in an uneroded mushy zone.

Since Eq (61) assumes a linear relationship between the interfacial drag and the velocity, it is only valid for creeping flow (i.e., for a Reynolds number based on the hydraulic radius of less than unity). Ganesan and Poirier (1990) include a second-order resistance term in Eq (61) that is proportional to the square of the velocity. This term only exists for anisotropic solid structures. On the other hand, Beckermann and Viskanta (1988) include a velocity square term to account for possible inertia (or "kinetic") effects on the interfacial stress. Their term is usually called Forchheimer's extension to Darcy's law and also exists for isotropic solid structures. In the porous-media literature, there has been an extensive discussion on the significance of such higher-order terms (Cvetkovic, 1986; Hassanizadeh and Gray, 1987; Barak, 1987; Hassanizadeh and Gray, 1988). At the present time, there is not sufficient experimental data to support the inclusion of velocity square terms in modeling of interfacial drag in mushy zones.

V.2 Calculation of the solid fraction

A main source of uncertainty and confusion in the use of the model presented in Sec V has been the calculation of the solid volume fractions, ε_α and ε_β. There are no equations that contain the volume fractions as the main dependent variable. Furthermore, in the mushy zone the energy and species conservation equations are intimately linked through the phase diagram relations and state functions given in Sec IV.3. Note that in the absence of convection and macroscopic solute diffusion, the species conservation equations and phase diagram relations can easily be combined to yield the well-known Lever rule or Scheil equation (Kurz and Fisher, 1989), which *are* explicit relations for the solid fraction. This is, however, not advisable in the presence of macroscopic solute transport (due to convection and diffusion).

Much research has recently been devoted to the development of efficient and fast algorithms to affect the coupling between the equations and "recover" the volume fractions (Prakash and Voller, 1989; Voller, 1990; Voller et al., 1990). One relatively general iterative procedure involves the following steps before the eutectic point in reached: (i) assume that the temperatures and concentrations (and, therefore, enthalpies) are known in the energy equation, Eq (58), and solve it for the solid fraction, ε_α or ε_β, (ii) solve the species conservation equations, Eqs (50) to (52) for the various average concentrations, taking the most recent values for the volume fractions and interfacial concentrations (or temperature), (iii) update the temperature from the phase diagram relations and go back to step (i). During the eutectic reaction, the α- and β-phases form simultaneously. Then, both the temperature and liquid concentration are at fixed values given by the phase diagram, so that the total solid fraction $\varepsilon_s = \varepsilon_\alpha + \varepsilon_\beta$ can be determined from the energy equation and ε_α or ε_β from the liquid species conservation equation. In practice, there are many important details to this procedure to affect fast convergence, and the reader is referred to a recent review (Voller et al., 1990) that covers both finite difference and finite element methods.

VI. PROGRESS TOWARDS A COMPREHENSIVE MODEL FOR COLUMNAR AND EQUIAXED SOLIDIFICATION

This section addresses modeling of solidification systems where columnar and equiaxed microstructures exist simultaneously. A combined columnar and equiaxed solid structure can be found in many casting processes (Flemings, 1974) and also occurs in magmatic systems (Loper and Roberts, 1978). The system considered is similar to the one shown in Fig 4. We also relax all assumptions made in Sec V regarding the microscopic processes. In other words, all phase interactions occurring on a microscopic scale are explicitly considered and separate conservation equations are utilized for each phase. This allows, for example, for the inclusion of nucleation, microsegregation, thermal and

solutal undercooling and solid movement. As mentioned in Sec II, all of these effects have a pronounced influence on the compositional and structural properties of a solidified alloy and should be included in a comprehensive model. Furthermore, the model provides a more general macroscopic framework than Eq (1) for the inclusion of microscopic processes.

The following discussion should not be viewed as a complete and final theory, but rather as an overview of the progress (or lack thereof) that has been made and of the various modeling aspects that need to be addressed both theoretically and experimentally. For conciseness, only one solid ($k=s$) and one liquid ($k=\ell$) phase are considered. The macroscopic conservation equations for each phase can be found in Table 1 and are not repeated here. As is evident from Sec IV, a two-phase model requires specification of the interfacial drag and heat and mass transfer coefficients (or diffusion lengths), the interfacial area ($A_s=A_\ell=A_i$) per unit volume (V_o), and the macroscopic viscosities, thermal conductivities, and mass diffusivities for each phase. Each of these quantities is addressed in the following sections.

VI.1 Interfacial transfers

Interfacial drag

It is customary to model the dissipative part of the interfacial stress, M_k^d, of the *solid* phase for moving solid particles (e.g., small equiaxed crystals) and of the *liquid* phase for flow through a fixed solid structure (e.g., columnar crystals or packings of equiaxed crystals) (Hassanizadeh and Gray, 1980; Drew, 1983). The interfacial drag needs to be modeled for one phase only, because the one for the other phase can be obtained from the interfacial momentum balance, Eq (23) (neglecting M_k^T). In solidification of alloys, there is a transition between moving and fixed solid structures. For example, with increasing solid volume fraction, equiaxed crystals will interact, pack, and eventually form a continuous solid structure. It is, therefore, desirable to obtain a correlation for the resistance coefficient R_k as a function of the liquid volume fraction, covering small nuclei in the melt ($\varepsilon_\ell \rightarrow 1$) as well as low permeability dendritic meshworks ($\varepsilon_\ell < 0.5$). Agarwal and O'Neill (1988) recently presented such a generalized drag coefficient model, and compared available theories for multi-particle systems. For an isotropic medium composed of spherical particles, the resistance coefficient R_k can be identified with a generalized drag coefficient, $C_{D\varepsilon}$, such that the interfacial drag is given by

$$M_s^d = \frac{3}{4}\frac{\varepsilon_s}{d_s}\rho_\ell\, C_{D\varepsilon}|<v_\ell>^\ell-<v_s>^s|\,(<v_\ell>^\ell - <v_s>^s)$$

(64)

where d_s is a mean particle length (diameter for spherical particles) of the solid phase that can be related to the interfacial area concentration, $S_v = A_i/V_o$, as

$$d_s = 6\varepsilon_s/S_v$$

(65)

The drag coefficient, $C_{D\varepsilon}$, is calculated as a function of a particle Reynolds number via

$$C_{D\varepsilon} = 24/(2\,Re\,C_{k\varepsilon}\varepsilon_s)$$

(66)

where $C_{k\varepsilon}$ is a generalized Kozeny coefficient and the particle Reynolds number Re is given by

$$Re = \varepsilon_s\rho_s\,|<v_\ell>^\ell - <v_s>^s|\,d_s/\mu_\ell$$

(67)

Since equiaxed crystals can generally be expected to have a small particle Reynolds number, inertia terms are not included in the expression for the drag coefficient.

For the packed bed regime ($\varepsilon_\ell < 0.5$), $C_{k\varepsilon}$ can be obtained by comparison with the Blake-Kozeny equation (see Sec VI and Bird et al., 1960), to give

$$C_{k\varepsilon} \approx 5$$

(68)

It is easily shown that Eqs (64) to (68), together with the interfacial momentum balance given by Eq (23), are mathematically identical to the permeability model given by Eqs (61) and (62). The Blake-Kozeny equation has also been found to work well for packings of equiaxed crystals (Murakami and Okamoto, 1984).

For the free particle regime ($\varepsilon_\ell > 0.5$), Agarwal and O'Neill (1988) recommend the following expression

$$C_{k\varepsilon} = \frac{1}{2}\frac{\varepsilon_\ell^3}{1-\varepsilon_\ell}\left[\frac{1 + 4.7\,(1-\varepsilon_\ell)}{1 - 1.83\,(1-\varepsilon_\ell)}\right]$$

(69)

For comparison, the well-known Richardson and Zaki (1954) model gives

$$C_{k\varepsilon} = \frac{1}{2}\frac{\varepsilon_\ell^{-1.65}}{1-\varepsilon_\ell}$$

(70)

In the limit of $\varepsilon_\ell \rightarrow 1$, Eqs (64) to (67) and (69) reduce to Stokes' law for a single particle (see Bird et al., 1960). At $\varepsilon_\ell = 0.5$, according to Eqs (68) and (69), there is a small discontinuity in the generalized Kozeny coefficient $C_{k\varepsilon}$ that causes the drag coefficient and, hence, the pressure drop to increase in the transition from the free particle to the packed bed regime (Andersson, 1961).

The above drag coefficient model, like the permeability model, needs experimental calibration, in order to relate the characteristic length scale d_s to (known) microstructural parameters. Presently, it is not at all clear how the multiple length scales present, for example, in equiaxed dendritic growth (i.e., the grain diameter, the dendrite tip radius, and the dendrite arm spacings) can be incorporated into the above correlation framework (which was originally developed for solid spheres). Nevertheless, West (1985), who proposed a

similar extension of the permeability model to high liquid fraction mushy zones, was able to obtain a good fit of the permeability data measured by Piwonka and Flemings (1966) over the entire liquid fraction range. Generally, little data is available for liquid fractions greater than 0.8. Some guidance may be obtained from studies of crystallization of various salt-water solutions (e.g., Ishii et al., 1977) and from the snow literature (e.g., List and Schemenauer, 1971) (snow crystals can be dendritic). Drag coefficient measurements during settling of various models of equiaxed dendrites and dendrite fragments have recently been performed by Zakhem et al. (1992) and correlated by Ahuja et al. (1992).

Interfacial heat and species transfer

(a) *Liquid side*. The inclusion of thermal $(T_{li} \neq <T_l>^l)$ and, particularly, solutal $(C_{li} \neq <C_l>^l)$ undercooling in the liquid is necessary for the prediction of microstructure formation in alloy solidification (Rappaz, 1989). As already mentioned, equiaxed growth would be impossible without undercooling of the liquid. Similarly, the phenomenon of recalescence commonly observed in castings is directly related to undercooling. In the interdendritic region the interfacial area concentration, $S_v = A_i/V_o$, is so large that the liquid can safely be assumed to be thermally and solutally well mixed (i.e., the undercoolings vanish). The crucial areas are the dendrite tips and eutectic growth fronts in both columnar and equiaxed growth. According to Eqs (25) and (26), modeling of undercooling requires specification of the interfacial heat and mass transfer coefficients (or diffusion lengths) and the interfacial area concentration (see below).

In the limiting case of diffusion dominated heat and species transfer in the liquid and assuming some idealized geometry, the temperature and solute gradients at the solid/liquid interface and, hence, the diffusion lengths, ℓ_l^q and ℓ_l^j, can be evaluated by solving the (exact) diffusion equations on a microscopic scale. Most analyses assume a quasi-steady state, which limits them to low growth rates. In the simplest of all cases, a spherical grain growing into an infinite liquid, the diffusion lengths are given by $\ell_l^q = \ell_l^j = d_s/2$. Models for dendrite tips are typically based on the Ivantsov solution for an isolated paraboloid (see Kurz and Fisher, 1989). This solution needs to be supplemented by an interface stability criterion in order to yield unique relationships. It is beyond the scope of this review to provide any details of the diffusion models that are available for a wide variety of (idealized) microstructures and the reader is referred to Kurz and Fisher (1989) and Thevoz and Rappaz (1991) for an up-to-date account. Rappaz (1989) reviewed, in addition, a number of models for multiple crystals, that take into account the finite extent of the liquid region around each crystal and impingement. As discussed in Sec III. these models have provided for quite realistic predictions of undercooling phenomena and microstructure formation on the system scale for purely diffusional transport.

The diffusional theories are of little use when convection is present. Nonetheless, convective heat and mass transfer coefficients have rarely been measured. Some data is available for equiaxed crystals grown from aqueous solutions (e.g., Palermo and Grove, 1964; Hayakawa and Matsuoka, 1973), which is relevant to industrial crystallizers used in the chemical industry (these crystals are not dendritic). While generalized correlations for heat and mass transfer coefficients that cover the entire liquid fraction range exist (Agarwal, 1988), they need to be adapted to the microstructures present in alloy solidification. Heat and mass transfer coefficients should be measured particularly for equiaxed crystals and columnar dendrite tips. Promising experimental methods include the use of transparent model alloys and optical diagnostic techniques (McCay et al., 1991) and Magnetic Resonance Imaging (Georgiadis, 1991). It should be noted that measurements at *single* dendrite tips [see Glicksman et al. (1986)] would not be directly useful, because of interference of the thermal and solutal fields from adjacent crystals and because the averaging volume contains several crystals. This issue is presently the main roadblock towards modeling of solidification with thermal and solutal undercooling. Besides dendritic growth, more research attention is also required for eutectic growth fronts with convection.

(b) *Solid side*. Modeling of finite rate solute diffusion in the solid on a microscopic scale is important for the prediction of microsegregation in the solidified alloy. In addition, both the interfacial heat and species transfer rates on the solid side of the solid/liquid interface influence the phase-change rates via the interfacial energy and solute balances (see Table 1 and below). Because heat and species transfer are analogous, the following discussion focuses on solute diffusion only.

Modeling of microsegregation is an extensive and active research area (see, for example, Yeum et al., 1989; Battle and Pehlke, 1990) and it is not possible to provide a review here. For dendritic solidification, Ohnaka (1986) has presented an elegant model that gives good agreement with experimental measurements and fits well into the present modeling framework. Ohnaka simply assumes a parabolic solute profile in the dendrite, so that the diffusion length is given by

$$\ell_s^j = \frac{d_s/2}{2 + n} \tag{71}$$

where $n = 1$, 2, or 3 for planar, cylindrical, or spherical geometries, respectively. Furthermore, Ohnaka assumes certain interface geometries. For example, for a square arrangement of the dendrite arms on a cross-sectional view of the averaging volume, we can write immediately

$$d_s = \lambda \, \varepsilon_s \tag{72}$$

and [compare to Eq (65)]

$$S_v = A_i/V_O = 4\varepsilon_s/\lambda , \tag{73}$$

where λ is a *mean* dendrite arm spacing. Equations (71) to (73) constitute a complete model for the interfacial solute transfer rate on the solid side, J_s^i, given by Eq (26). Upon making a number of other simplifying assumptions (which have no direct relevance to the present discussion), Ohnaka (1986) is able to obtain an analytical solution for the solid fraction variation with local temperature in the mushy zone that accounts for finite rate solute diffusion in the solid. More importantly, Ohnaka found that the solution is not too sensitive to the assumed dendrite shape and growth mode. The major discrepancy with experimental data occurs for $\varepsilon_s > 0.9$. This may be attributed to the neglect of dendrite arm coarsening (i.e., λ was assumed constant) and the reduction in the interfacial area due to impingement and merging of solid/liquid interfaces (this is discussed in the next section), as well as to the assumption of a time-independent, parabolic solute profile. While the above model can certainly be improved upon, it illustrates the basic procedures (and problems) for incorporating finite rate solute (and heat) diffusion in the solid on a microscopic scale into macroscopic conservation equations and interfacial balances. Note that this model of finite rate species diffusion in the solid on a microscopic scale can also be incorporated into the macroscopic solid species conservation equations presented in Sec V [i.e., Eqs (51) and (52)].

Topological relations

The previous two subsections show that the interfacial area concentration, $S_v = A_i/V_O$, is an important parameter in the modeling of the interfacial transfer terms. From a physical point of view, the interfacial area concentration contains the information regarding the geometry of the interfaces that is lost through the averaging process. This information plays an important part in the behavior of a solidifying system and must be restored through a constitutive relation. As noted by Boure (1987), the knowledge of the average motion of the interface alone (i.e., $\overline{w}_{ns}$) does not suffice to determine the variation of the interfacial area concentration. This variation also depends on the geometry (topology) of the interface.

The interfacial area concentration (as well as ε_s) can be measured by quenching and sectioning the material at a preselected time during the solidification process. S_v is equal to twice the number of intersections of a random test line with the interface on a 2-D cross section, per unit length of the test line. Then, a mean characteristic length (diameter) of the solid microstructure can be calculated from (DeHoff and Rhines, 1968; Bird et al., 1960)

$$d_s = 6\varepsilon_s/S_v . \tag{74}$$

Much additional research is necessary before a topological relation for S_v can be specified. An illustration of the basic

dependence of S_v on ε_s is provided in Fig 7. In general, S_v is a function of the number of crystals per unit volume, n, according to (DeHoff and Rhines, 1968)

$$S_v \sim n^{1/3} . \tag{75}$$

The calculation of n is discussed in more detail in Sec VI.3. For columnar dendritic growth, n can be viewed as the number density of primary arms, so that $n^{1/3} \sim 1/\lambda_1$. The primary arm spacing, λ_1, may, in turn, be related to the local solidification conditions (Kurz and Fisher, 1989). During solidification of a given averaging volume, S_v increases from zero, eventually reaches a maximum value and then decreases again to zero because of merging of the solid/liquid interfaces and impingement. This behavior may be modeled using the empirical relation given by Speich and Fisher (1966)

$$S_v \sim \varepsilon_s (1 - \varepsilon_s) . \tag{76}$$

This relation cannot be used for $\varepsilon_s < 0.02$ and $\varepsilon_s > 0.95$, because $dS_v/d\varepsilon_s$ should be infinitely large at $\varepsilon_s = 0$ and 1. Furthermore, coarsening experiments at a constant solid fraction have shown that the interfacial area concentration decreases according to (Marsh et al., 1988)

$$S_v \sim t_\alpha^{-1/3} , \tag{77}$$

where t_α is the local "aging" time. At the present, it is not clear how the above descriptions can be incorporated into a single topological relation for a given metal alloy. Neglecting impingement, Eq (73) may give a reasonable estimate of S_v in a dendritic mushy zone, provided the mean dendrite arm spacing, l, can be calculated in a meaningful way (that may include coarsening).
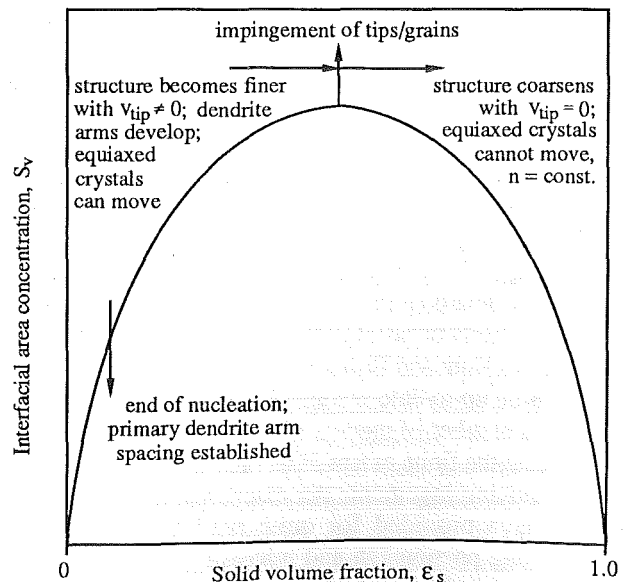

FIG 7.   Illustration of the dependence of the interfacial area concentration on the solid volume fraction (Ni et al., 1991).

VI.2 Macroscopic transport coefficients

Viscosities

Much has been said about the (mixture) viscosity and rheology of suspensions and slurries (Krieger, 1972; Jeffrey and Aarivos, 1976; Darby, 1986). However, the use of separate momentum equations in a two-phase model requires the specification of both the effective liquid and solid viscosities over the entire solid fraction range. A very approximate model is presented in the following, in order to illustrate the basic ideas and the problems encountered.

For small (spherical) nuclei in the melt, such that $\varepsilon_s \to 0$, we can write (Nunziato, 1983)

$$\mu_\ell^* = \mu_\ell \qquad\qquad (\varepsilon_s \to 0) \qquad\qquad (78)$$

and

$$\mu_s^* = 3.5\mu_\ell \qquad\qquad (\varepsilon_s \to 0) . \qquad\qquad (79)$$

The finite solid viscosity arises from collisions between the particles. The above form of Eq (79) arises from Einstein's theory for dilute suspensions of spheres. Einstein (1905) actually derived an expression for the suspension or mixture viscosity, μ_m, as

$$\mu_m = (1 + 2.5\ \varepsilon_s)\ \mu_\ell . \qquad\qquad (80)$$

For very small particles, we have $\langle v_\ell \rangle^\ell = \langle v_s \rangle^s$, so that

$$\mu_m = \varepsilon_s \mu_s^* + \varepsilon_\ell \mu_\ell^* . \qquad\qquad (81)$$

Then, by substituting Eqs (80) and (78) into Eq (81) and solving for μ_s^*, we obtain Eq (79).

In the other extreme, for flow through a rigid solid structure, such as a columnar mushy zone and packings of equiaxed crystals, we found in Sec V that

$$\mu_\ell^* = \mu_\ell \qquad\qquad \text{(rigid solid)} \qquad\qquad (82)$$

provides at least for a first approximation. Therefore, it is proposed to take Eqs (78) or (82) for all solid fractions and structures. Furthermore, for rigid solid structures we take

$$\mu_s^* \to \infty \qquad\qquad \text{(rigid solid)} . \qquad\qquad (83)$$

This "forces" the macroscopic velocity gradients of the solid phase to vanish. If the rigid solid structure is attached to a wall, the solid velocity will then be uniformly equal to the velocity of the wall (which may be zero). For equiaxed solidification, we need a smooth transition between Eqs (79) and (82), because equiaxed crystals form a rigid solid structure only above a certain solid fraction, ε_s^c, which depends on the microstructure. Dendritic crystals will form a

rigid structure once the dendrite arms interlock and the dendrite tip movement has ceased, such that the entire volume is occupied by an open solid structure. Depending on the solidification conditions, the corresponding value of ε_s^c can vary from about 0.1 up to at most 0.6 (Rappaz and Thevoz, 1987). For granular (or globulitic) crystals, a value of approximately 0.6 has been reported for ε_s^c (Murakami and Okamoto, 1984), which corresponds well to the maximum value of ε_s for a random packing of spheres. The transition in the macroscopic solid viscosity may be achieved by using Krieger's (1972) model for the mixture viscosity of concentrated suspensions, i.e.,

$$\mu_m = \mu_\ell\ [1 - \varepsilon_s/\varepsilon_s^c]^{-2.5\varepsilon_s^c} \qquad\qquad (84)$$

substituting it into Eq (81) and solving for μ_s^*. Note that Eq (84) together with Eq (81) reduces to Eq (79) for $\varepsilon_s \to 0$ and to Eq (84) for $\varepsilon_s \ge \varepsilon_s^c$. Obviously, this procedure is questionable, because for $0 < \varepsilon_s \le \varepsilon_s^c$, $\langle v_s \rangle^s$ is generally not equal to $\langle v_\ell \rangle^\ell$. However, it does provide for a smooth transition between the two extreme values for μ_s^* in equiaxed solidification. Alternatively, one could assume that μ_s^* increases exponentially with ε_s. A more complicated model, based on kinetic theory, has recently been proposed by Ding and Gidaspow (1990).

Not covered by the above model is the non-Newtonian behavior that is exhibited by dense solid-liquid slurries (Soo, 1989). The non-Newtonian nature is evident by the fact that a finite shear stress must be applied to settled equiaxed crystals before they can move. However, this phenomenon is probably not too important in common casting processes. In so-called semisolid forming processes (Flemings, 1991), the relative movement between the solid and liquid can be neglected, so that a variety of non-Newtonian mixture viscosity models apply (see Darby, 1986).

Thermal conductivities and mass diffusivities

The effective (macroscopic) thermal conductivities and mass diffusivities for each phase should be obtained from measurements. As a first approximation, one may be tempted to take these effective coefficients equal to their microscopic counterparts. The validity of this assumption will depend on the grain structure. For example, it is not at all clear how to model the macroscopic solid diffusivities for small equiaxed crystals completely surrounded by melt. Microstructural dependencies in columnar growth have already been discussed in Sec V. Despite the importance of these issues, no measurements of the effective thermal conductivities and mass diffusivities as a function of the mushy zone morphology have been reported.

VI.3 Calculation of the solid fraction

In the model presented in Secs VI.1 and VI.2, the procedures for calculating the solid volume fraction, ε_s, are quite

different from those discussed in Sec V.2. The difference is not only due to the fact that the solid fraction may be advected with moving crystals, but also because the model of Sec VI accounts for thermal and solutal undercooling, and microscopic diffusion in the solid. In the absence of liquid and solid convection, the solid fraction models reviewed by Rappaz (1989) can be used [together with Eq (1)] to account for the above mentioned microscopic effects. However, with convection and in the framework of the single-domain equations of Sec VI, the solid fraction calculation procedures need to be reconsidered.

Because we specified an explicit relation between the liquid and solid phase pressures (see Sec IV.2), the solid fraction can be calculated from the solid continuity equation, that is (see Table 1)

$$\frac{\partial}{\partial t}(\varepsilon_s \rho_s) + \nabla \cdot (\varepsilon_s \rho_s <v_s>^s) = S_v \rho_s \bar{w}_{ns} . \qquad (85)$$

The right hand side of Eq (85) accounts for the solid fraction variation due to phase change. It can be seen that during coarsening (when S_v decreases) at a constant solid fraction, the average velocity of the interface, $\bar{w}_{ns}$, is equal to zero. The second term on the left hand side of Eq (85) accounts for the solid fraction variation due to advective transport of solid.

The interfacial velocity $\bar{w}_{ns}$ is determined from the interfacial energy and species balances, which can now be written as (see Table 1 and the foregoing constitutive relations)

$$\Delta h \rho_s \bar{w}_{ns} = \frac{k_\ell}{\ell_\ell^q}(\bar{T}_i - <T_\ell>^\ell) + \frac{k_s}{\ell_s^q}(\bar{T}_i - <T_s>^s) \qquad (86)$$

and

$$(\bar{C}_{\ell i} - \bar{C}_{si})\rho_s \bar{w}_{ns} = \frac{\rho_\ell D_\ell}{\ell_\ell^j}(\bar{C}_{\ell i} - <C_\ell>^\ell)$$

$$+ \frac{\rho_s D_s}{\ell_s^j}(\bar{C}_{si} - <C_s>^s) \qquad (87)$$

where $\Delta h = \bar{h}_{\ell i} - \bar{h}_{si}$ is the latent heat of fusion. Note that the terms in the parentheses on the right hand side of Eqs (86) and (87) are the thermal and solutal undercoolings, respectively. The intrinsic volume averaged temperatures and species concentrations (or enthalpies) are determined from the solution of the macroscopic conservation equations for each phase. Then, together with the phase diagram relations, the above interfacial balances can be solved simultaneously for the interfacial temperatures and species concentrations, as well as for $\bar{w}_{ns}$.

The calculation of the interfacial area concentration, S_v, in the presence of solid movement can be further illuminated by writing the solid fraction as $\varepsilon_s = n V_{sc}$, where V_{sc} is the solid volume of a single crystal. Substitution into Eq (85) yields after a few steps

$$\frac{\partial n}{\partial t} + \nabla \cdot (<v_s>^s n)$$

$$= \frac{S_v}{V_{sc}}\bar{w}_{ns} - \frac{n}{\rho_s V_{sc}}\left[\frac{\partial \rho_s V_{sc}}{\partial t} + <v_s>^s \cdot \nabla(\rho_s V_{sc})\right]$$

$$= \dot{n} . \qquad (88)$$

The left hand side of Eq (88) shows that the number density of crystals is conserved so that the right hand side was set equal to the net generation rate of crystals, $\dot{n}$. The net generation rate includes both the "birth" and "death" of crystals due to nucleation, dendrite arm remelting, agglomeration and other effects. Whereas nucleation has received considerable research attention (Flemings, 1974; Kurz and Fisher, 1989), it is not clear how to model the other modes of crystal generation in the presence of convection. It can be said that realistic modeling of grain structure formation in castings will depend to a large extent on resolving this issue (Steube and Hellawell, 1992). Equation (88) can, theoretically, be solved for the crystal density, n. Recall that n is an important parameter in the topological relation for the interfacial area concentration, S_v (see Sec VI.1).

Since there presently exist considerable uncertainties in the modeling of the interfacial transfer terms, special care must be taken in calculating the solid fraction. For limiting values of certain parameters in the interfacial transfer terms, the solid fraction should take the correct values corresponding, for example, to the cases of complete thermal equilibrium within V_o, complete chemical equilibrium (i.e., no species concentration gradients) in the liquid phase and no species diffusion in the solid, or complete mixing of the species in both phases. Fortunately, this can be achieved through proper numerical solution procedures (Spalding, 1983).

VII. DISCUSSION AND CONCLUSIONS

A mathematical modeling framework for alloy solidification is reviewed that attempts to take into account the many ways in which microscopic phenomena influence transport processes on a macroscopic scale. Both, the more simple model presented in Sec V and the complete two-phase model of Sec VI require considerable amounts of additional research. In this respect, modeling of nucleation and interfacial drag and heat and mass transfer in the presence of convection, as well as of dispersion (turbulence) and the macroscopic material coefficients should receive particular attention. Although these are very complicated issues, they do represent the *next* generation of problems in solidification modeling. The feasibility and success of comprehensive models is amply demonstrated by the micro-/macroscopic modeling efforts recently reported in the literature (Rappaz, 1989; Stefanescu et al., 1990; Goettsch and Dantzig, 1991; Chang et al., 1992; Loser and Herlach, 1992) and continued progress in modeling of other multi-phase systems. The

importance of closely coupled experimental and theoretical research cannot be overemphasized. Aside from the more fundamental aspects discussed here, numerous problems also exist in the numerical implementation of the equations and the practical application of the models to real solidification processes (Viskanta, 1991). Other shortcomings of present theories of transport phenomena in solidification and the need for *future* generation models is briefly discussed in the following.

Although the *effects* of microscopic phenomena are reflected in the present modeling framework, the equations cannot be utilized to *predict* microstructure formation. In other words, the constitutive relations rely to a large extent on an *a prior* knowledge of the structures and transport phenomena present on a microscopic scale. This problem can be linked to the lack of sufficient resolution provided by the volume averaging approach. As noted in Sec II, in order to predict the formation of microstructures, it is particularly important to account for the special growth conditions of dendrite tips and eutectic fronts. However, averaging volumes containing such tips or fronts always have *multiple* length scales. For example, for an averaging volume with several equiaxed dendritic crystals, one can identify at least three different microscopic length scales that are all much smaller than the averaging volume: (i) the overall radius of the crystal, (ii) the radius of the dendrite tips, and (iii) the secondary arm spacing. Consequently, the interfacial fluxes and the interface velocities are highly non-uniform in such averaging volumes. Obviously, these complicated microscopic phenomena are not well characterized by the use of a single *mean* characteristic length, *mean* interfacial fluxes, and a single *mean* interfacial velocity for a given averaging volume. This leaves the question open how, for example, the mean length is related to the multiple lengths of the actual microstructure.

In the micro-macroscopic models of Dustin and Kurz (1986) and Rappaz and Thevoz (1987) for equiaxed dendritic solidification, better resolution is obtained through the use of two separate volume fractions for the averaging volume: the fraction of grains in the liquid and the internal solid fraction within the grain. This way, one is able to distinguish between the different phenomena associated with the dendrite tip region and the interdendritic region. The total volume of the solid in the averaging volume is then simply equal to the product of the grain fraction and internal solid fraction. Such an analysis requires separate interfacial balances for the grain and the averaging volume.

From a fundamental point of view, we are dealing with a *heterogeneous* multi-phase system having multiple and disparate length scales. In order to capture the effects of the heterogeneities, one could use multiple averaging volumes of different sizes or, more generally, spatial homogenization procedures (Bensoussan et al., 1978). Some progress in this direction has recently been made in the area of two-phase flow in heterogeneous porous media (Quintard and Whitaker, 1988). Due to the dynamic nature of solidification, one may also have to resort to averaging volumes of non-constant

size (Gray, 1983). Work is underway to apply these concepts to solidification (Wang and Beckermann, 1992).

ACKNOWLEDGEMENTS

REFERENCES

Agarwal P (1988), Transport Phenomena in Multi-particle System - II. Particle-Fluid Heat and Mass Transfers, *Chem Eng Sci* **43**(9), 2501-2510.

Agarwal P and O'Neill B (1988), Transport Phenomena in Multi-Particle System - I. Pressure Drop and Friction Factors: Unifying the Hydraulic-Radius and Submerged-Object Approaches, *Chem Eng Sci* **43**(9), 2487-2499.

Ahuja S, Beckermann C, Zakhem CR, Weidman PD, and deGroh III HC (1992), Drag Coefficient of an Equiaxed Dendrite Settling in an Infinite Medium, in *Micro-Macro Scale Phenomena in Solidification*, C Beckermann, LA Bertram, SJ Pien, and RE Smelser (eds), ASME Publication, New York NY.

Andersson KB (1961), Pressure Drop in Ideal Fluidization, *Chem Eng Sci*, **15**, 276-297.

Battle TP, and Pehlke RD (1990), Mathematical Modeling of Microsegregation in Binary Metallic Alloys, *Metall Trans B* **21B**, 357-375.

Barak AZ (1987), Comments on 'High Velocity Flow in Porous Media' by Hassanizadeh and Gray, *Transport Porous Media* **2**, 533-535.

Beckermann C (1987), Melting and Solidification of Binary Mixtures with Double-Diffusive Convection in the Melt, *PhD Thesis*, Purdue University, West Lafayette IN.

Beckermann C and Viskanta R (1988), Double-Diffusive Convection during Dendritic Solidification of a Binary Mixture, *PhysicoChem Hydrodyn* **10**(2), 195-213.

Beckermann C and Ni J (1992), Modeling of Equiaxed Solidification with Convection, in *Proceedings of International Conference on Transport Phenomena Processing*, Technomic, PA.

Bennon WD and Incropera FP (1987), A Continuum Model for Momentum, Heat and Solute Transfer in Binary Solid-Liquid Phase Change Systems - I. Model Formulation, *Int J Heat Mass Transfer* **30**(10), 2161-2170.

Bensoussan A, Lions LL, and Papanicolaou G (1978), *Asymptotic Analysis for Periodic Structures*, North-Holland, New York.

Bird RB, Steward WE, and Lightfoot EN (1960), *Transport Phenomena*, John Wiley, New York NY.

Boure JA (1987), Two-Phase Flow Models: The Closure Issue, in Multiphase Science and Technology Vol. 3, GF Hewitt, JM Delhaye, and N Zuber (eds), Hemisphere, Washington DC.

Chang S, Shangguan D, Stefanescu, DM (1992), Modeling of the Liquid/Solid and the Eutectoid Phase Transformations in Spheroidal Graphite Cast Iron, *Metall Trans A* **23A**, 1333-1346.

Copley SM, Giamei AF, Johnson SM, and Hornbecker MF (1970), The Origins of Freckles in Unidirectionally Solidified Castings, *Metall Trans* **1**, 2193-2204.

Cvetkovic VD (1986), A Continuum Approach to High Velocity Flow in a Porous Medium, *Transport Porous Media* **1**, 63-97.

Darby R (1986), Hydrodynamics of Slurries and Suspensions, in Encyclopedia of Fluid Mechanics **5**, NP Cheremisionoff (ed), Gulf Publishing Company, Houston TX.

deGroh III HC and Laxmanan V (1988a), Bulk Undercooling, Nucleation, and Macrosegregation of Pb-Sn Alloys, *Metall Trans A* **19A**, 2651-2658.

deGroh III HC and Laxmanan V (1988b), Macrosegregation in Undercooled Pb-Sn Eutectic Alloys, in Solidification Processing of Eutectic Alloys, DM Stefanescu, GJ Abbaschian, and RJ Bayuzick (eds), Metallurgical Society, Warrendale PA, 229-242.

DeHoff RT and Rhines FN (1968), *Quantitative Microscopy*, McGraw-Hill, New York.

Ding J and Gidaspow D (1990), A Bubbling Fluidization Model Using Kinetic Theory of Granular Flow, *AIChE Journal* **36**(4), 523-538.

Drew DA (1983), Mathematical Modeling of Two-Phase Flow, *Ann Rev Fluid Mech*, **15**, 261-291.

Durand F (1992), Convective Effects on the Solidification Grain Structure, presented at *NATO Advanced Research Workshop on Interactive Dynamics in Convection and Solidification*, Chamonix, France, March.

Dustin I and Kurz W (1986), Modeling of Cooling Curves and Microstructures during Equiaxed Dendritic Solidification, *Z Metallkd*, **77**, 265-273.

Einstein A (1905), On the Movement of Small Particles Suspended in a Stationary Liquid Demanded by the Molecular-Kinetic Theory of Heat, *Annln Phys*, **17**, 549.

Felicelli SD, Heirich JC, and Poirier DR (1991), Simulation of Freckles during Vertical Solidification of Binary Alloys, *Metall Trans B* **22B**, 847-859.

Flemings MC (1974), *Solidification Processing*, McGraw-Hill, New York.

Flemings MC (1991), Behavior of Metal Alloys in the Semisolid State, *Metall Trans B* **22B**, 269-293.

Flemings MC and Nereo GE (1967), Macrosegregation Part I, *Trans AIME* **239**, 1449-1461.

Flemings MC and Nereo GE (1968b), Macrosegregation Part III, *Trans AIME* **242**, 50-55.

Flemings MC, Mehrabian R, and Nereo GE (1968a), Macrosegregation Part II, *Trans AIME* **242**, 41-49.

Flood SC and Hunt JD (1987), Columnar and Equiaxed Growth, *J Crystal Growth* **82**, 543-551.

Flood, SC, Katgerman L, and Voller VR (1991), The Calculation of Macrosegregation and Heat and Fluid Flows in the DC Casting of Aluminium Alloys, in *Modeling of Casting, Welding and Advanced Solidification Processes -V*, M Rappaz, MR Ozgu, and KW Mahin (eds), TMS, Warrendale PA, 683-690.

Fujii T, Poirier PR, and Flemings MC (1979), Macrosegregation in a Multi-Component Low Allow Steel, *Metall Trans B* **10B**, 331-339.

Ganesan S and Poirier DR (1990), Conservation of Mass and Momentum for the Flow of Interdendritic Liquid during Solidification, *Metall Trans B* **21B**, 173-181.

Ganesan S, Chan CL, and Poirier DR (1992), Permeability for Flow Parallel to Primary Dendrite Arms, *Mater Sci and Eng* **A151**, 97-105.

Georgiadis JG (1991), Future Research Needs in Convective Heat and Mass Transport in Porous Media, in *Convective Heat and Mass Transfer*, S Kakac (ed), Kluwer, Dordrecht, Netherlands, **E196**, 1073-1088.

Glicksman ME, Coriell SR, and McFadden GB (1986), Interaction of Flows with the Crystal-Melt Interface, *Ann Rev Fluid Mech* **18**, 307-335.

Goettsch DD and Dantzig JA (1991), Modeling Microstructure Development in Gray Iron Castings, in *Modeling of Casting and Welding and Advanced Solidification Processes -V*, M Rappaz, MR Ozgu, and KW Mahin (eds), TMS, Warrendale PA, 377-385.

Gray WG (1975), A Derivation of the Equations for Multi-Phase Transport, *Chem Eng Sci* **30**, 229-233.

Gray WG (1983), Local Volume Averaging of Multiphase Systems Using a Non-Constant Averaging Volume, *Int J Multiphase Flow* **9**(6), 755-761.

Hassanizadeh M and Gray WG (1979a), General Conservation Equations for Multi-Phase Systems: 1. Averaging Procedure, *Adv Water Resources* **2**, 131-144.

Hassanizadeh M and Gray WG (1979b), General Conservation Equations for Multi-Phase Systems: 2. Mass, Momenta, Energy, and Entropy Equations, *Adv Water Resources* **2**, 191-203.

Hassanizadeh M and Gray WG (1980), General Conservation Equations for Multi-Phase Systems: 3. Constitutive Theory for Porous Media Flow, *Adv Water Resources* **3**, 25-40.

Hassanizadeh M and Gray WG (1987), High Velocity Flow in Porous Media, *Transport Porous Media* **2**, 521-531.

Hassanizadeh M and Gray WG (1988), Reply to Comments by Barak on 'High Velocity Flow in Porous Media' by Hassanizadeh and Gray, *Transport Porous Media* **3**, 319-321.

Hassanizadeh M and Gray WG (1990), Mechanics and Thermodynamics of Multiphase Flow in Porous Media Including Interphase Boundaries, *Adv Water Resources* **13**(4).

Hayakawa T and Matsuoka M (1973), Effect of Heat Transfer on Crystal Growth for Inorganic Salt-Water Systems, *Heat Transfer -Japan* **2**(2), 104-115.

Hills RN, Loper DE, and Roberts PH (1983), A Thermodynamically Consistent Model of a Mushy Zone, *Quart J Mech and Appl Math* **36**, 505-536.

Huppert HE (1990), The Fluid Mechanics of Solidification, *J Fluid Mech* **212**, 209-240.

Incropera FP, and Viskanta R (1992), Effects of Convection on the Solidification of Binary Mixtures, in *Heat Transfer and Mass Transfer in Material*, I Tanasawa and N Lior (eds), Hemisphere, Washington DC, 295-312.

Ishii M (1975), *Thermo-Fluid Dynamic Theory of Two-Phase Flow*, Eyrolles, Paris.

Ishii T, Fujita S, and Johnson AI (1977), Continuous Multi-Particle Crystal Growth in Vertical Cones, *Canadian J Chem Eng* **55**, 177-184.

Jeffrey DJ and Aarivos A (1976), The Rheological Properties of Suspensions of Rigid Particles, *AIChE* **22**, 417-432.

Kato H and Cahoon JR (1985), Inverse Segregation in Directionally Solidified Al-Cu-Ti Alloys with Equiaxed Grains, *Metall Trans A* **16A**, 579-587.

Krieger IM (1972), Rheology of Monodispersed Latices, *Advan Colloid Interface Sci* **3**, 111-136.

Kurz W and Fisher DJ (1989), *Fundamentals of Solidification*, Trans Tech Publications, Aedermannsdorf, Switzerland.

Langer JS (1989), Dendrites, Viscous Fingers, and the Theory of Pattern Formation, *Science* **243**, 1150-1156.

Larson RE and Higdon JJL (1986), Microscopic Flow Near the Surface of Two-Dimensional Porous Media. Part 1. Axial Flow, *J Fluid Mech* **166**, 449-472.

Lesoult G (1991), Prediction of Cast Structures, Segregations, and Defects: Progresses and Tendencies, in Modeling of Casting and Welding and Advanced Solidification Processes -V, M Rappaz, MR Ozgu, and KW Mahin (eds), TMS, Warrendale, PA, 363-375.

List R and Schemenauer RS (1971), Free-Fall Behavior of Planar Snow Crystals, Conical Graupel and Small Hail, *J Atmos Sci* **28**, 110-115.

Loper DE and Roberts PH (1978), On the Motion of an Iron-Alloy Core Containing a Slurry. I. General Theory, *Geophys Astrophys Fluid Dyn* **9**, 298-321.

Loser W and Herlach DM (1992), Theoretical Treatment of the Solidification of Undercooled Fe-Cr-Ni Melts, *Metall Trans A* **23A**, 1585-1591.

Lundgren TS (1972), Slow Flow through Stationary Random Beds and Suspensions of Spheres, *J Fluid Mech* **51**, 273-299.

Marsh SP, Glicksman ME, Meloro L, and Tsutsumi K (1988), Thermal and Microstructure Characteristics of Mushy Zones, in *Modeling and Control of Casting and Welding Processes IV*, AF Giamei and GJ Abbaschian (eds), TMS, PA, 15-23.

McCay T, McCay M, and Hopkins J (1991), Dendrite Tip Thermal and Solutal Conditions Measured during Directional Solidification, *AIAA Paper* No. 1333.

Mehrabian R, Keane M, and Flemings MC (1970), Interdendritic Fluid Flow and Macrosegregation: Influence of Gravity, *Metall Trans* **1**, 1209-1220.

Murakami K and Okamoto T (1984), Fluid Flow in the Mushy Zone Composed of Granular Grains, *Acta Metall* **32**(10), 1741-1744.

Murphy DW, Johnson DW, Jin S, and Howard RE (1988), Processing Techniques for the 93K Superconductor $Ba_2 YCu_3 O_4$, *Sci* **241**, 922-930.

Neale G and Nader W (1974), Practical Significance of Brinkman's Extension of Darcy's Law: Coupled Parallel Flows within a Channel and a Bounding Porous Medium, *Canadian J Chem Eng* **52**, 475-478.

Ni J and Beckermann C (1990), A Two-Phase Model for Mass, Momentum, Heat, and Species Transport during Solidification, Transport Phenomena in *Material Processing*, M Charmchi, MK Chyu, Y Joshi, and SM Walsh (eds), ASME, HTD-VOL. 132, New York, 45-56.

Ni J and Beckermann C (1991), A Volume-Averaged Two-Phase Model for Transport Phenomena during Solidification, *Metall Trans B* **22B**, 349-361.

Ni J, Feller RJ, and Beckermann C (1990), A Two-Phase Model of Transport Phenomena during Solidification, presented at the *Conference on Modeling of Casting, Welding and Advanced Solidification Processes*, Engineering Foundation Conference, Davos, Switzerland, Sept. 16-21.

Nunziato JW (1983), A Multiphase Mixture Theory for Fluid-Particle Flows, in *Theory of Dispersed Multiphase Flow*, RE Meyer (ed), Academic Press, New York, 191-226.

Ohnaka I (1986), Mathematical Analysis of Solute Redistribution During Solidification with Diffusion, *Iron Steel Inst Japan* **26**(12), 1045-1051.

Ohno A (1987), *Solidification*, Springer, Berlin.

Oldenburg CM and F J Spera (1992), Hybrid Model for Solidification and Convection, *Numer Heat Transfer* **21**(B), 217-229.

Palermo JA and Grove CS (1964), Some Variables Affecting the Rate of Crystal Growth in Aqueous Solutions, *AIChE* **10**(3), 351-356.

Patankar SV (1982), *Numerical Heat Transfer and Fluid Flow*, Hemisphere, New York.

Pines V, Zlatkowski M, and Chait A (1990), Time Development of a Perturbed-Spherical Nucleus in a Pure Supercooled Liquid. II. Nonlinear Development, *Phys Review A* **42**(10), 6137-6150.

Piwonka TS and Flemings MC (1966), Pore Formation in Solidification, *TMS-AIME* **236** 1157-1165.

Poirier DR (1987), Permeability for Flow of Interdendritic Liquid in Columnar-Dendritic Alloys, *Metall Trans B* **18B**, 245-255.

Poirier DR and Nandapurkar P (1988), Enthalpies of a Binary Alloy during Solidification, *Metall Trans A* **19A**, 3057-3061.

Poirier DR, Nandapurkar PJ, and Ganesan S (1991), The Energy and Solute Conservation Equations for Dendritic Solidification, *Metall Trans B* **22B**, 889-900.

Prakash C (1990a), Two-Phase Model for Binary Solid-Liquid Phase Change, Part I: Governing Equations, *Numer Heat Transfer Part B* **18**, 131-145.

Prakash C (1990b), Two-Phase Model for Binary Solid-Liquid Phase Change, Part II: Some Illustrative Examples, *Numer Heat Transfer Part B*, **18**, 147-167.

Prakash C and Voller VR (1989), On the Numerical Solution of Continuum Mixture Model Equations Describing Binary Solid-Liquid Phase Change, *Numer Heat Transfer Part B* **15**, 171-189.

Prantil VC and Dawson PR (1983), Application of a Mixture Theory to Continuous Casting, in *Transport Phenomena in Materials Processing*, MM Chen, J Mazumder and CL Tucker III (eds), ASME, New York, 469-484.

Prescott PJ and Incropera FP (1991), Numerical Simulation of a Solidifying Pb-Sn Alloy: The Effects of Cooling Rate on Thermosolutal Convection and Macrosegregation, *Metall Trans B* **22B**, 529-540.

Prescott PJ, Incropera FP, and Bennon WD (1991), Modeling of Dendritic Solidification Systems: Reassessment of the Continuum Momentum Equation, *Int J Heat Mass Transfer* **34**(9), 2351-2359.

Prescott PJ, Incropera FP, and Gaskell DR (1992), The Effects of Undercooling, Recalescence and Solid Transport on the Solidification of Binary Metal Alloys, presented at *28th National Heat Transfer Conference*, ASME, New York.

Quintard M, and Whitaker S (1988), Two-Phase Flow in Heterogeneous Porous Media: The Method of Large-Scale Averaging, *Transport Porous Media* **3**, 357-413.

Rappaz M, and Stefanescu DM (1988), Modeling of Equiaxed Primary and Eutectic Solidification, in *Solidification Processing of Eutectic Alloys*, DM Stefanescu, GJ Abbaschian, and RJ Bayuzick (eds), TMS, Warrendale, PA, 133-151.

Rappaz M and Thevoz Ph (1987), Solute Diffusion Model for Equiaxed Dendritic Growth, *Acta Metall* **35**(7), 1487-1497.

Rappaz M (1989), Modelling of Microstructure Formation in Solidification Processes, *Int Mater Rev* **34**, 93-123.

Rappaz M and Voller VR (1990), Modeling of Micro-Macrosegregation in Solidification Processes, *Metall Trans A* **21A**, 749-753.

Richardson JF and Zaki WN (1954), Sedimentation and Fluidisation: Part I, *Trans Instn Chem Eng* **32**, 35-53.

Ridder SD, Kou S, and Mehrabian R (1978), Effects of Fluid Flow on Macrosegregation in Axisymmetric Ingots, *Metall Trans B* **9B**, 435-447.

Roberts PH and Loper DE (1987), Dynamic Processes in Slurries, in *Structure and Dynamics of Partially Solidified Systems*, DE Loper (ed), NATO ASI Series, Nijhoff, Dordrecht, 229-290.

Rohatgi P (1988), Foundry Processing of Metal Matrix Composites, *Modern Casting* April, 1988, 47-50.

Sahm PR, Jones H, and Adam CM (1986), *Science and Technology of the Undercooled Melt*, NATO ASI Series, Nijhoff, Dordrecht.

Sahraoui M and Kaviany M (1991), Slip-and No-Slip Boundary Conditions at Interface of Porous, Plain Media, in *Proceedings of the ASME/JSME Thermal Engineering Conference Vol. 4*, ASME, New York, 273-286.

Sample AK and Hellawell A (1984), The Mechanism of Formation and Prevention of Channel Segregation during Alloy Solidification, *Metall Trans A* **15A**, 2163-2173.

Schneider M and Beckermann C (1991), Effects of Simplified Enthalpy Relations on Prediction of Heat Transfer during Solidification of a Lead-Tin Alloys, *Appl Math Modelling* **15**, 596-605.

Schneider MC (1991), Modeling the Columnar Dendritic Solidification of Lead-Tin Alloys, *MSME. Thesis*, The University of Iowa, Iowa City IA.

Sekhar JA and Dantzig JA (1991), Nature and Properties of Semi-Solid Materials, TMS, Warrendale PA, 1991.

Sha WT, Chao BT, and Soo SL (1984), Porous-Media Formulation for Multiphase Flow with Heat Transfer, *Nucl Eng and Des* **82**, 93-106.

Slattery JC (1967), Flow of Viscoelastic Fluids through Porous Media, *AIChE* **13**, 1066-1071.

Soo SL (1989), *Particulates and Continuum: Multiphase Fluid Dynamics*, Hemisphere, New York.

Spalding DB (1983), Developments in the IPSA Procedure for Numerical Computation of Multiphase-Flow Phenomena with Interphase Slip, Unequal Temperatures, Etc, in *Numerical Properties and Methodologies in Heat Transfer*, TM Shin (ed), Hemisphere, Washington DC.

Speich GR, and Fisher RM (1966), Recrystallization of a Rapidly Heated 31/4% Silicon Steel, Recrystallization, in *Grain Growth and Textures*, ASM, Metal Park OH, 563-598.

Stefanescu DM, Curreri PA, and Fiske MR (1986), Microstructural Variations Induced by Gravity Level during Directional Solidification of Near-Eutectic Iron-Carbon Type Alloys, *Metall Trans A* **17A**, 1121-1130.

Stefanescu DM, Upadhya G, and Bandyopadhyay D (1990), Heat Transfer-Solidification Kinetics Modeling of Solidification of Castings, *Metall Trans A* **21A**, 997-1005.

Steube RS and Hellawell A (1992), An Alternative Approach to Modeling the Grain Structure of Castings, in *Micro-Macro Scale Phenomena in Solidification*, C Beckermann, LA Bertram, SJ Pien, and RE Smelser (eds), ASME, New York.

Szekely J and Jassal AS (1978), An Experimental and Analytical Study of the Solidification of a Binary Dendritic System, *Metall Trans B*, **9B**, 389-398.

Thevoz Ph, Desbiolles JL, and Rappaz M (1989), Modeling of Equiaxed Microstructure Formation in Casting, *Metall Trans A* **20A**, 311-322.

Thevoz Ph and Rappaz M (1991), Modelling of Equiaxed Microstructures in Solidification Processes: An Overview of Solute Diffusion Models, in *Modeling of Casting, Welding and Advanced Solidification Processes - V*, M Rappaz, MR Ozgu, KW Mahin (eds), TMS, Warrendale PA, 387-394.

Viskanta R (1990), Mathematical Modeling of Transport Phenomena during Solidification of Binary Systems, presented at *22nd Int Center Heat Mass Trans. Symposium on Manuf and Mat Processing*, Dubrovnik, Yugoslavia, August 27-31.

Viskanta R (1991), Materials Processing: Structural Materials, in *Report of a NSF Thermal Sciences Workshop on Thermal Sciences: Emerging Technologies and Critical Phenomena*, HR Jacobs and JP Hartnett (eds), Chicago IL, April.

Viskanta R and Beckermann C (1987), Mathematical Modeling of Solidification, in *Interdisciplinary Issues in Materials Processing and Manufacturing*, SK Samanta, R Komanduri, R McMeeking, MM Chen, and A Tseng (eds), ASME, New York, 501-526.

Voller VR (1990), Fast Implicit Finite Difference Method for the Analysis of Phase Change Problems, *Numer Heat Transfer B* **17**, 155-169.

Voller VR and Prakash C (1987), A Fixed Grid Numerical Modelling Methodology for Convection-Diffusion Mushy Region Phase-Change Problems, *Int J Heat Mass Transfer* **30**(8), 1709-1719.

Voller VR, Brent AD, and Prakash C (1989), The Modelling of Heat, Mass and Solute Transport in Solidification Systems, *Int J Heat Mass Transfer* **32**(9), 1719-1731.

Voller VR, Brent AD, and Prakash C (1990), Modeling the Mushy Region in a Binary Alloy, *Appl Math Modelling* **14**, 320-325.

Voller VR, Stachowicz MS, and Thomas BG (1991), *Materials Processing in the Computer Age*, TMS, Warrendale PA.

Voller VR, Swaminathan CR, and Thomas BG (1990), Fixed Grid Techniques for Phase Change Problems: A Review, *Int J Numer Methods in Eng* **30**, 875-898.

Voller VR (1992), Effect of Solidification Morphology on the Macroscopic Behavior of Solidification Systems, presented at *NATO Advanced Research Workshop on Interactive Dynamics in Convection and Solidification*, Chamonix, France.

Wang CY and Beckermann C (1992), A Multiphase Micro-Macroscopic Model of Solute Diffusion in Dendritic Alloy Solidification, in *Micro-Macro Scale Phenomena in Solidification*, C. Beckermann, LA Bertram, SJ Pien, and RE Smelser (eds), ASME, New York.

West R (1985), On the Permeability of the Two-Phase Zone during Solidification of Alloys, *Metall Trans A* **16A**, 693.

Whitaker S (1967), Diffusion and Dispersion in Porous Media, *AIChE* **13**, 420-427.

Yeum KS, Laxmanan V, and Poirier DR (1989), Efficient Estimation of Diffusion during Dendritic Solidification, *Metall Trans A* **20A**, 2847-2856.

Yoo H and Viskanta R (1992), Effect of Anisotropic Permeability on the Transport Processes during Solidification of a Binary Mixture, *Int J Heat Mass Transfer*, (in press).

Zakhem R, Weidman PD, and deGroh H (1992), On the Drag of Model Dendrite Fragments at Low Reynolds Number, presented at *International Conference on Transport Phenomena in Processing*, Hawaii.

Raymond Viskanta *received a BS in Mechanical Engineering from the University of Illinois in 1955 and an MSME and PhD from Purdue University in 1956 and 1960, respectively. After working at Argonne National Lab he joined the faculty of Purdue as an Associate Professor in 1962 and was promoted to Professor in 1966. He was named Goss Distinguished Professor of Engineering at Purdue in 1986. His current research interests include heat transfer and combustion systems, melting and solidification of materials, transport in porous media, buoyancy driven convection flow and heat transfer, heat transfer related to materials processing and radiative transfer in participating media. He has been active in the committees of ASME and AIAA and is currently the Technical Editor of ASME Journal of Heat Transfer. His awards include: ASME Heat Transfer Memorial Award; AIAA Thermophysics Award; ASEE Senior Research Award; Purdue Chapter Sigma Xi Research Award; ASME/AIChE Max Jakob Memorial Award; ASME Heat Transfer Best Paper Award; ASME Melville Medal; Nusselt-Reynolds Prize of the Assembly of World Conferences on Experimental Heat Trnasfer, Fluid Mechanics and Thermodynamics, and member of the National Academy of Engineering, foreign member of the Lithuanian Academy of Sciences, US Senior Scientist Award from the Alexander von Humboldt Foundation, and Fellowship Award from the Japan Society for the Promotion of Science.*

Christoph Beckermann *recieved a Vordiplom in mechanical engineering from the University of Hannover, West Germany in 1981. In 1984 and 1987, he received MS and PhD degrees in mechanical engineering from Purdue University. He joined the faculty of the Department of Mechanical Engineering at the University of Iowa in 1987 as an Assistant Professor and was promoted to Associate Professor in 1992. Dr Beckermann was the recipient of a Fulbright Fellowship (1982), a Herrick Laboratories Fellowship (1982-1984), a Quadrille Ball Committee Scholarship of teh Germanistic Society of America (1985), a University of Iowa Old Gold Summer Fellowship (1988), a National Science Foundation Presidential Young Investigator Award (1989), and a Certificate of Appreciation from the Materials Division of ASME. He spent the fall of 1992 at the Foundry-Institute, RWTH Aachen, Germany. Dr. Beckermann's current research interests include solidification of materials, transport in porous media, and natural convection heat and mass transfer. At present, he is a member of the Committee on Heat Transfer in Manufacturing and Materials Processing of the ASME Heat Transfer Division. He is the author of 28 refereed journal papers and 17 conference presentations.*